DEVELOPMENT OF A STIMULI-RESPONSIVE, HYDROLYSABLE POLY(VINYL LAURATE-*co*-VINYL ACETATE) NANOPARTICLE PLATFORM FOR THE SLOW AND CONTROLLED IN-SITU RELEASE OF SURFACTANTS

A Thesis

Presented to the Faculty of Graduate School

of Cornell University

in Partial Fulfillment of the Requirements for the Degree of

Master of Science

by

Bashayer Saad A Aldakkan

August 2021

ABSTRACT

Efficient surfactant delivery with controlled release is of great practical interest in various fields including oil spill remediation and oil recovery.[1–3] Premature adsorption of surfactants at various surfaces and interfaces reduces their efficiency and limits practical applications. To alleviate this challenge, nanoencapsulation methods have been proposed and, in most systems, the immobilization relies on relatively weak, noncovalent interactions between the surfactant molecules and the host, which leads to premature release.[4–6]

In this study, a stimuli-responsive, sub-100nm nanoparticle platform with a hydrolysable ester side chain for in-situ generation of surfactants is demonstrated. The nanoparticles serve as a delivery vehicle as well as a precursor for the surfactant derived from the pendant ester groups. The nanoparticles, ~ 55 nm in diameter with a zeta potential of -54 mV, were synthesized via copolymerization of vinyl-laurate and vinyl-acetate (p-(VL-co-VA), 3:1 molar ratio) as the core and stabilized with a protective poly(ethylene-glycol) (PEG) shell. Hydrolysis kinetics in an accelerated, base-catalysed reaction show release of about 11 and 31% of available surfactant in DI water at 25 and 80°C, respectively. The corresponding values in saline water are 22 and 76%. The efficiency of the released surfactant in reducing the interfacial tension (IFT), altering wettability, stabilizing an oil-water emulsion, and generation of foam was investigated through spinning drop tensiometer (SDT) analysis, contact angle measurements, laser confocal scanning microscopy (LCSM) imaging and dynamic foamability assessment, respectively. The performance was benchmarked to sodium laurate (SL), a commercially available surfactant. The system was further investigated for targeted

delivery of surfactants to the oil phase by grafting poly(glycidyl methacrylate), PGMA, brush on the surface. The collective findings of the study demonstrate both the efficacy of the NP system to produce surfactants in-situ and the ability to manipulate and control various interfacial phenomena including wettability, emulsions, and foams.

BIOGRAPHICAL SKETCH

Bashayer Aldakkan is from Riyadh, Saudi Arabia. She obtained her Bachelor of Science Degrees in Chemical Engineering and Economics from the Pennsylvania State University in 2016. Prior to joining the MSE MS program at Cornell, Bashayer worked at Saudi Aramco's upstream research center (EXPEC Advanced Research Center) focusing on production enhancement technologies related to stimulation and fracturing fluids. She also worked as a reservoir engineer in Khurais field during the increment project and as a production engineer.

To my beloved parents; Nora and Saad,

And my siblings; Abdulrahman, Sattam, Faisal & Bdour

And my dearest friend; Sarah

For their unconditional love, support, and encouragement.

ACKNOWLEDGMENT

List of Figures

13

List of Tables

1. CHAPTER 1: INTRODUCTION

This chapter discusses the motivation of surfactant delivery in a wide range of fields and the specific scope of this work in relation to Enhanced Oil Recovery (EOR) applications.

1.1 Motivation of Surfactant Delivery and Objective

Surfactants have been extensively researched and are indispensable in a wide spectrum of industries including manufacturing[7–9] pharmaceuticals,[10–12] oil recovery,[3,13,14] detergency,[15,16] and the food industry.[17,18] A practical challenge with surfactant deployment is that they are susceptible to fast adsorption at various surfaces and interfaces, which limits their effectiveness.[19] In oil reservoirs, deposition of heavy organic matter and polar components alters the wettability of the oil-bearing formation from an originally water-wet to a heterogenous strongly oil-wet or mixed-wet state.[20] Surfactant-assisted flooding is widely used as a chemical stimulant to alter wettability, lower the oil-water interfacial tension (IFT) and create emulsions/foams to boost oil production.[3] However, designing an optimized and cost-effective surfactant flood remains a challenge due to the operational challenges associated with premature adsorption at the rock surface, pore blockage and scaling/corrosion tendencies.[3] Surfactant retention is a term used to refer to the amount of surfactant adsorbed in the rock and it depends on the characteristics of the rock and type of surfactant utilized. It is preferable to achieve a low retention rate (<1 mg/g of rock).[21,22] To alleviate surfactant loss due to adsorption and increased retention rates, sacrificial chemicals (e.g. polymers) have been explored but they lead to high implementation costs and associated formation damage in Enhanced Oil Recovery (EOR) applications.[23,24] Nano-encapsulated systems have been investigated as an alternative method for efficient surfactant delivery.

However, challenges remain with the easy dissociation of surfactant molecules from the nanoparticle host attributed to the anchoring mechanism between the surfactant and the capsule through weak, noncovalent interactions such as hydrogen bonding, van der Waals, electrostatic or hydrophobic/hydrophilic interactions.[25] In this regard, the ability to design a stimuli-responsive, hydrolysable nanoparticle template as the delivery vehicle and the surfactant precursor offers significant potential in deep treatment delivery for oil recovery and environmental remediation.[1,26]

1.2   Scope of work

Herein, a new surfactant delivery platform based on hydrolysable polymeric nanoparticles is reported. The system consists of polymeric nanoparticles, which serve as a delivery vehicle as well as a precursor for the surfactant. More specifically, the nanoparticles consist of hydrolysable poly(vinyl laurate-co-vinyl acetate), P(VL-co-VA), core that are either grafted with; (1) a poly(ethylene glycol) (PEG) shell, or (2) a poly(glycidyl methacrylate) (PGMA) brush. The PEG serves as a protective shell for a controlled, slow-release profile while the PGMA brush is designed to enhance the stability and the responsiveness for the system for targeted delivery of surfactant to the oil phase in oil-water mixtures.

The release mechanism involves slow hydrolysis of the pendant ester group to generate carboxylic acid, which subsequently reacts with the carbonate surface to produce carboxylate salts. The hydrolysis kinetics and the surfactant release profile at varying pH, salinity and temperatures were systematically studied using a base-catalyzed reaction. The rate of surfactant release measured by an accelerated alkaline-assisted hydrolysis test using 0.1M and 1M sodium hydroxide (NaOH) demonstrate a

slow-release profile. Contact angle measurements were utilized to evaluate the surfactancy in altering the wetting state of an oil-saturated calcite substrate. Confocal microscopy images demonstrate the effectiveness of the hydrolyzed nanoparticles to stabilize oil/water emulsions. Foamability of the NPs to enhance gas flooding operations and promotion of conformance control was assessed by dynamic foam analysis. Finally, interfacial Tension (IFT) measurements were conducted to isolate the individual contributions from the neat, *unhydrolyzed* P(VL-co-VA) NPs and the *hydrolyzed* P(VL-co-VA) NPs.

The study further explores the potential of PGMA tethering on the surface to enhance the stability in high salinity environment and allow the system to be used for targeted delivery application. This approach capitalizes on the facile conversion of the epoxy groups into functional moieties yielding a polymeric brush with multiple charges for electrostatic and steric stabilization.

2. CHAPTER 2: BACKGROUND

2.1 Surfactant Advances and Prospects

Surfactants are one of the most versatile products in a wide range of technological applications.[7-19] Their amphiphilic structure consists of a hydrophilic polar group attached to a hydrophobic tail with varying lengths, branching and saturation. The opposing polarity of the surface-active molecules and preferential segregation at solid-liquid and liquid-liquid interfaces marks their significance in a diverse range of surface and interfacial phenomena, such as wetting, emulsions, foaming, and detergency. [27,28,29] The following sections discuss surfactants adsorption behavior that controls a variety of interfacial processes.

2.1.1 Wetting Modifications by Surfactants

Wetting is defined as the ability of a fluid to sustain contact with a solid surface by the formation of intermolecular interactions, resisting the displacement by other fluids.[29,30] The surface and interfacial tension between a solid substrate (adsorbent) and the spreading fluid (adsorbate) can be inferred from the contact angle (θ), which is defined as the mechanical equilibrium of a drop influenced by three interfacial tensions; (i) liquid-vapor (γ_{lv}), (ii) solid-liquid (γ_{Sl}), (iii) solid-vapor (γ_{Sv}), defined by Young's Equation:[31]

$$\gamma_{lv} \cos(\theta) = \gamma_{Sv} - \gamma_{Sl} \tag{1}$$

It is of great practical interest to reduce the contact angle and adhesion on hydrophobic surfaces, which are widely utilized as glass covers for solar cells, microfluidics and automobiles.[32] Typically, water does not spontaneously spread over hydrophobic surfaces due to the high surface tension (γ_{lv}) of 72 mN/m at

25°C.[33] Thus, under certain conditions, the utilization of surfactants is prompted to reduce the triad interfacial tensions between the substrate and the aqueous solution and alter the wettability. For polar substrates, wettability alteration through surfactants can be achieved via different mechanisms depending on the surfactant end charge.[34] Surfactants of opposite charge to the substrate will tend to adsorb on the surface with the hydrophilic-end oriented at the interface and the hydrophobic-tail in the aqueous solution, reducing γ_{sl}. The ion-pair formation accelerates oil desorption and allow for spontaneous aqueous imbibition into the substrate matrix to restore a water-wet state. On the contrary, surfactants with the same charge as the adsorbent orient at the solid surface through the hydrophobic tail, while the hydrophilic head groups create a water-wet state layer on the surface (Figure 1).[35]
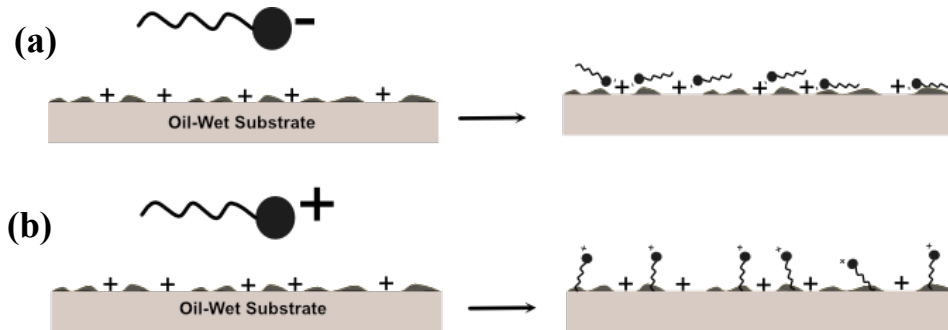
Figure 1 Surfactant adhesion onto charged, oil-wet substrate (a) electrostatic interactions between the opposite charges of surfactants and the substrate, (b) the hydrophobic interaction between the hydrophobic tail and the oil in the substrate.

The presence of electrolytes plays a prominent effect on the performance of the surface-active agents and their influence on the interfacial tensions as well as on their characteristic critical micelle concentration (CMC).[36,37,38] For example, short-hydrophobic chain length surfactants (C7-C8 carbon chain lengths) demonstrate better performance in solutions with high ionic strengths.[29]

2.1.2 Emulsification by Surfactants

Emulsification of two immiscible phases is widely investigated in many scientific disciplines related to colloidal systems, polymer science and interfacial processes.[39] Unlike microemulsions, the typical formation of oil-in-water or water-in-oil macroemulsions comprise the formation of large droplets that are unstable with high excess Gibbs free energy per drop that cannot be counteracted by entropy.[40] Enhancing the thermodynamic stability of emulsions and/or the creation of microemulsions facilitates advancements in several technological fields including drug delivery systems,[41] oil spillage remediation, [42] improving the mobility ratio in oil recovery,[43] and in chemical synthesis.[44]

Surface forces play a prominent effect in the stabilization of emulsions, hence, the utilization of surfactants are considered as they adsorb at the liquid-liquid interface reducing interfacial tension between the two immiscible phases and minimize the energy required for emulsification.[45] Surfactants also play a pivotal role in electrostatic, mechanical or steric stabilization of droplets, which hinders coalescence of the dispersed phase.[46] Surfactants can be combined with active solid particles, such as silica, carbon and polymer latexes, to create suspoemulsions with synergistic enhancement to emulsion stability.[47,48] In addition to the CMC, surfactant intrinsic characteristics must be considered when using them as emulsifying agents. For example, the hydrophilic to the lipophilic balance (HLB) determined their surface activity and tendency to assemble at the interface with no preferential solubility in either of the two bulk phases.[49]

2.1.3 Foaming and Antifoaming by Surfactants

Foams, or gas emulsions, are defined as the nonequilibrium dispersion of gas bubbles in a continuous liquid or solid phase separated by thin films (lamellae).[50] The utilization of surfactants as foaming agents is assessed through; (i) foam production ability defined as the initial height of foam produced and (ii) foam stability defined by the differential foam height after a given amount of time.[51] In foaming liquids, foam collapse is influenced by gravitational drainage of the liquid in the lamellae, coalescence of bubbles with close proximity, and differential osmotic and Laplace pressures relating to gas concentration and interfacial tension, respectively.[52] The difference in gas pressure of two adjacent bubbles is defined as the Laplace pressure, ΔP:

$$\Delta P = \gamma \left(\frac{1}{R_1} + \frac{1}{R_2} \right) \qquad (2)$$

where γ is the surface tension of the liquid, R_1 and R_2 are the radii of the gas bubble. As described below surfactant interfacial packing in an essential ingredient in the stabilization of liquid foams providing reduced surface tension, increased Electrostatic Double Layer (EDL),[53] and enhanced Gibbs elasticity and Marangoni effect initiating surface tension gradient of the two phases.[54]

2.1.3.1 Surface Tension Reduction

The preferential adsorption of surfactants at the liquid-vapor interface prompts favorable energetics that reduce the interfacial energy per unit area.[55] This sole effect is insufficient in providing foam stability, however, it facilitates less mechanical energy needs in creating large interfacial areas in foams.

2.1.3.2 Electrostatic Double Layer (EDL)

To offset film thinning due to attractive van der Waals interactions between bubbles, surface-active molecules provide a balancing repulsive force through the Electrostatic Double Layer (EDL), which is a representation of the ionic environment in the vicinity of a charged surface. The EDL is highly influenced by the pH and ionic strength of the liquid.

2.1.3.3 Gibbs Elasticity and Marangoni Flows

Liquid membrane surrounding gas bubbles must possess film elasticity that can counterbalance a local thinning/stretching caused by an applied stress. Film elasticity can occur only in the presence of surface-active solutes,[29] and with the increase in surfactant concentration and packing fluctuation, a surface tension (σ) gradient is induced with area (A), which is quantified by Gibbs Elasticity, E:

$$E = \frac{d\sigma}{d\ln A} \tag{3}$$

The induced surface tension gradient promotes Marangoni flow of the liquid film to the direction with higher surface tension, where the fluid movement hinders the coalescence of gas bubbles.[56]

2.2 Surfactants in Enhanced Oil Recovery (EOR)

Current recovery factors of oil reserves is capped between 30-35% of the original-oil-in-place (OOIP) due to the complex interplay of geological, physical and economic factors.[57] Recovery techniques of oil reserves can be classified as either primary, secondary or tertiary (Enhanced Oil Recovery, EOR) (Figure 2). Primary depletion, which contributes to up to 20% of recovery, capitalizes on the natural energy of the subterranean reservoir in the extraction of oil to the surface or through the utilization of

artificial lifting systems.[58] Secondary recovery methods rely on an external fluid injection to compensate for the depleted reservoir force required for oil extraction, which is accomplished through either water flooding or gas flooding resulting in incremental recovery factors up to 40%.[58] Tertiary, or Enhanced Oil Recovery (EOR), methods promote favorable conditions to displace residual oil by enhanced interactions between the injected treatment and the oil/rock by thermal and non-thermal methods resulting in up to 60% of recovery.[59]
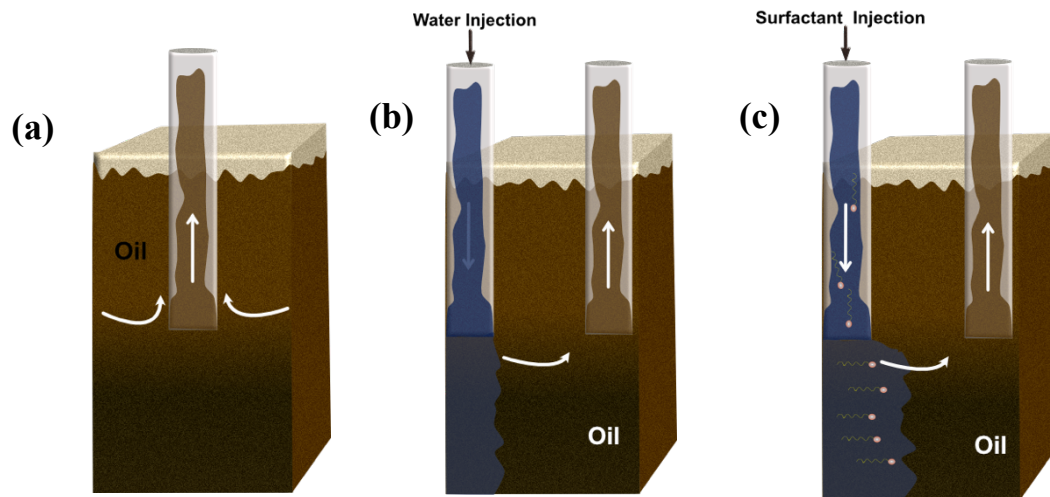
Figure 2 Recovery methods of oil reserves classified into (a) primary, (b) secondary, (c) tertiary (Enhanced Oil Recovery, EOR)

In petroleum-bearing formations, there is a preferential tendency for the oil phase to spread and adhere to the rock surface, effecting the relative permeability, capillary pressure and fluid distribution, which restricts residual oil production.[60] Thus, the deposition of heavy organic matter and polar components alters the wettability of the formation from an originally water-wet to a heterogenous strongly oil-wet or mixed-wet

state.[60] Typical waterflooding has been insufficient in naturally fractured, oil-wet formations with high contrast of permeability regions.[61] During water injection in an oil-wet formation, the high interfacial tension (IFT) between water and crude oil as the two immiscible phases results in a weak capillary force that is insufficient for oil displacement.[62] Waterflooding can also bypass residual oil due to the high water-to-oil mobility ratio, M:[63]

$$M = \frac{k_{rw}/\mu_w}{k_{ro}/\mu_o} \tag{4}$$

where k_{rw} and k_{ro} is the relative permeability of water and oil, respectively, and μ denotes the viscosity of the water or oil phases.

Thus, in an oil-wet, heterogenous formation matrix, a more involved approach is used, where surface-active agents are combined with polymers or alkali mixtures during waterflooding. Surfactant-assisted flooding acts as a chemical stimulant to alter wettability, lower oil-water interfacial tension (IFT) and create microemulsions/foams to increase the capillary force and lower the mobility ratio required to boost oil production.[3]

Subsurface surfactant delivery to enhance oil recovery in various types of reservoirs and more specifically carbonate reservoirs is limited by several technical and economic challenges. The heterogenous characteristics of the carbonate rock at different scales including pore, grain and texture that originated from the depositional history and diagenesis, create a complex pathway for fluid migration in the porous medium.[3] The following sections describe current surfactant delivery methods in a porous matrix.

2.2.1 Batch Neat Surfactant Treatments

Batch surfactant delivery, comprising of either neat surfactants, alkaline-surfactant (AS) mixtures, surfactant-polymer slugs or a combination thereof, are one of the widely used techniques in surfactant flooding.[64,65] To alleviate surfactant loss due to adsorption and increased retention inside the porous media, sacrificial chemicals (e.g. polyelectrolytes) have been explored, which lead to high implementation costs and associated formation damage in Enhanced Oil Recovery (EOR) applications.[23,24] Operational limitations such as low surfactant slug injecitivty, pumping failures, scaling/corrosion tendencies, pore blockage, premature surfactant adsorption and degradation of active agents at reservoir conditions have been widely experienced that necessitate continuous re-injection. [3,66,67]

2.2.2 Nano-Enabled Delivery: Inorganic Nanocapsules

One of the proposed methods to overcome the challenges associated with batch-surfactant flooding is developing a responsive nanoparticle system that can navigate through the porous media and is able to protect the surface-active agents against premature adsorption or degradation for deep treatment delivery. Inorganic nanoparticles have been widely investigated as delivery systems including carbon nanotubes (CNT),[68,69]noble metal NPs,[70,71]magnetic NPs (Fe_3O_4), zinc oxide (ZnO) NPs,[72]copper oxide (CuO) NPs,[73] titanium dioxide TiO_2 NPs,[74] and silica NPs.[75,] Thus far, TiO_2 NPs,[4] carbonaceous nanomaterials,[76] clay nanotubes,[77] Fe_3O_4 nanoparticles,[78] and silica nanoparticles[79] were investigated as inorganic carriers for efficient surfactant delivery in the recovery of oil. Nourafkan et al.[4] proposed porous TiO_2 as nanocarriers to deliver a blend of surfactant mixtures consisting of anionic alkyl aryl sulfonic acid (AAS) and nonionic alcohol ethoxylated (EA) surfactants. They reported a reduced

surface interaction of the surfactant molecules with the rock surfaces.[4] Chen et al.[76] investigated multi-walled nanotubes (MWNT) and carbon blacks (CB) in the encapsulation of alpha olefin sulfonate (AOS) surfactant. Mesoporous silica nanocarriers have been considered due to the effect of silanol groups in anchoring and immobilizing encapsulated organic compounds.[80] de Freitas and co-workers[6], for example, studied the encapsulation of diethanolamides (DEA) surfactants in SBA-15 silica nanoparticles and obtained enhanced retention in water and full release at oil/water interfaces. However, challenges with low surfactant effectiveness in such nano-encapsulated systems attributed to the anchoring mechanism within the nanoparticle pores through hydrogen bonding or weak van-der Waals interactions still persist.[25]

2.2.3   Nano-Enabled Delivery: Organic & Polymeric Nanoparticles

The facile desorption of surfactant molecules from the host in inorganic nanomaterials prompted the need for a delivery system that acts as a carrier and as a surfactant precursor. Organic and polymeric nanomaterials offer promising prospects in the petroleum field and have been only explored as encapsulating carriers for oil recovery applications. De Avila et al. proposed polystyrene nanoparticles (PSNP) in the encapsulation of ionic (sodium dodecyl sulfate, SDS) and nonionic (nonyl-phenol ethoxylate-10, NF-10EO) surfactants, that can be released by oil uptake-triggered swelling. [5] Rosestolato et al. explored the utilization of lipid nanostructures, comprised of beeswax (BW), to encapsulate nonylphenol ethoxylate (NPE10) surfactant triggering the release at the oil/water interface.[81]

To advance the delivery mechanism, a stimuli-responsive, hydrolysable polymeric nanoparticle template, which serve as a delivery vehicle as well as a precursor for the

surfactant is being investigated in this thesis. The potential of this work spans from surfactant delivery for oil recovery applications and oil spill remediation to surfactant therapies in drug delivery.[82]

3. CHAPTER 3: HYDROLYSABLE POLY(VINLY LAURATE-*co*-VINYL ACETATE) NANOPARTICLE PLATFORM

3.1 PREABLE

In this research, a surfactant precursor and a delivery platform based on hydrolysable nanoparticles is demonstrated. The nanoparticles consist of poly(vinyl laurate-co-vinyl acetate) core with two different grafting techniques; (i) polymerizable poly(ethylene glycol) (PPEG) protective shell (Figure 3) and (ii) glycidyl methacrylate (GMA) polymer brush (Figure 4). The release mechanism, as illustrated in Figure 5, involves slow hydrolysis of the ester group to generate carboxylic acid, which subsequently reacts with the carbonate surface to produce carboxylate salts. The hydrolysis kinetics and the surfactant release profile at varying pH, salinity and temperatures were systematically studied. The ratio of monomers as well as the PEG length or GMA grafting density were optimized to achieve colloidal stability while ensuring proper hydrolysis rate of the ester side chain. The study represents a step forward in the ability to manipulate and control oil-water interfaces and might pave the way for practical solutions in a number of important applications.
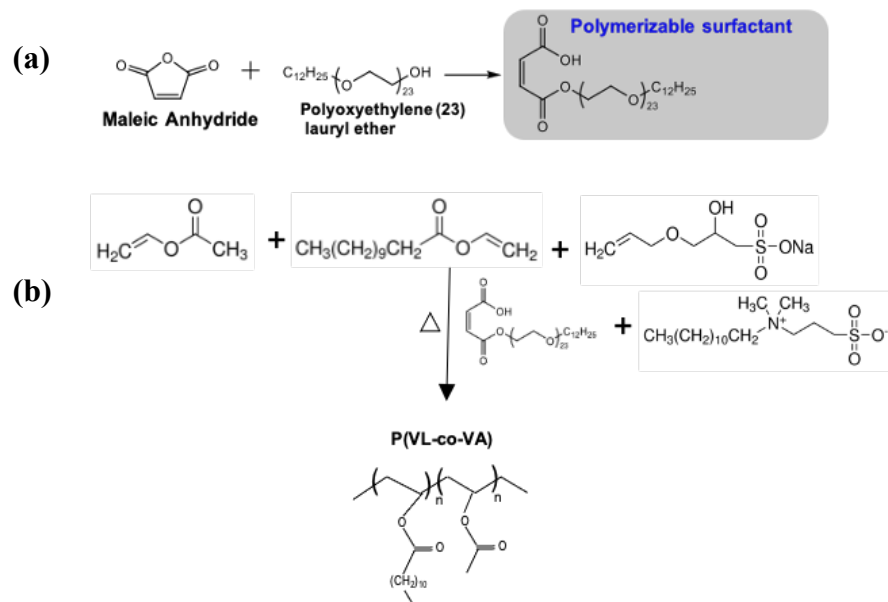
Figure 3 Synthesis scheme of (a) Polymerizable PEG (PPEG) precursor, and (b) P(VL-co-VA) NPs

(a)
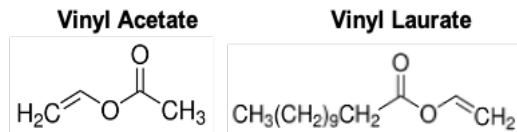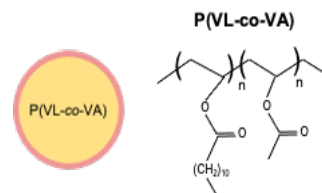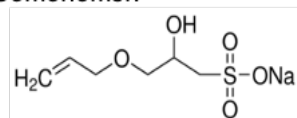
Monomers:
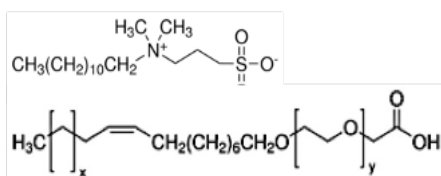
(b)
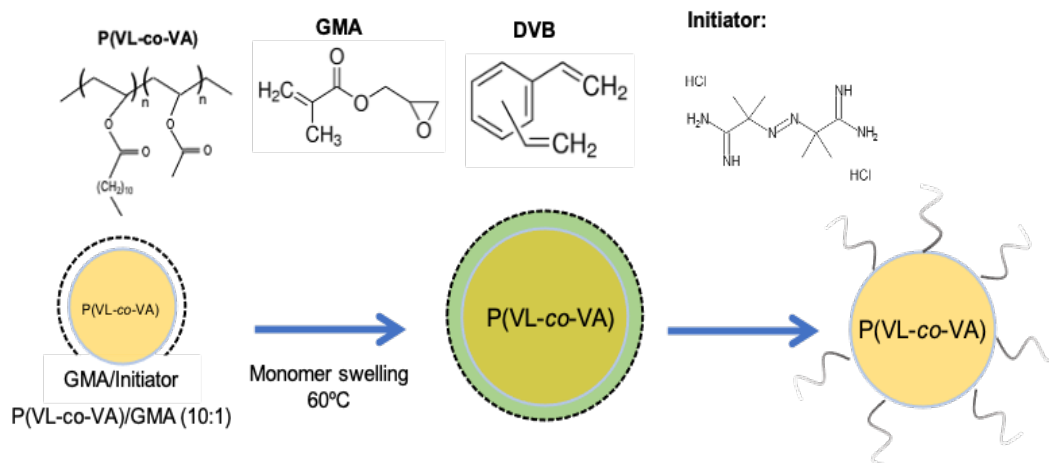
Figure 4 Synthesis scheme of (a) P(VL-co-VA) NPs core and (b) glycidyl methacrylate (GMA) polymer brush.
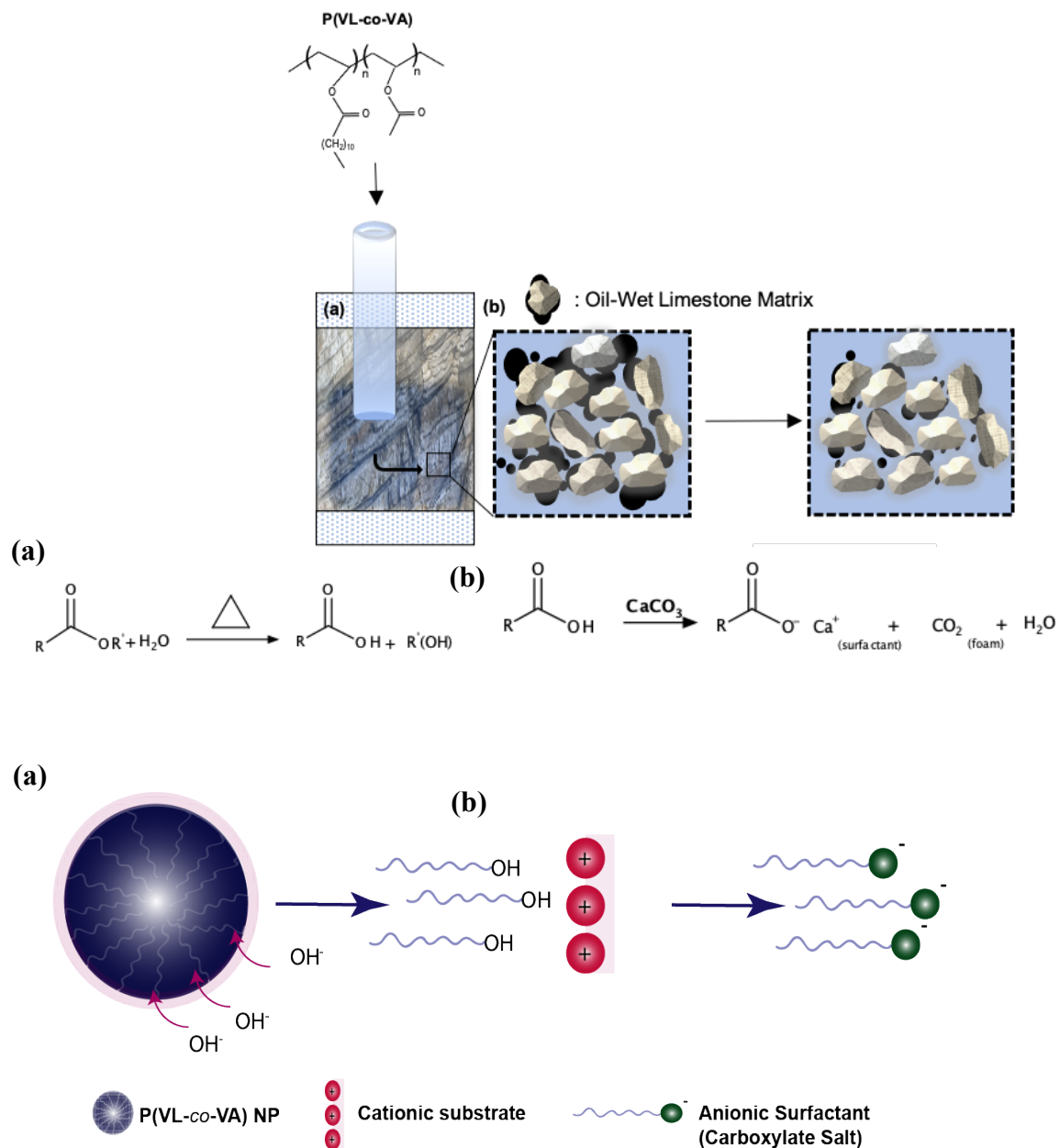
Figure 5 Hydrolysis mechanism of the injected P(VL-co-VA) nanoparticles in displacing residual oil from a limestone reservoir matrix. (a) hydrolysis activation to generate carboxylic acid, (b) carboxylic acid deprotonation and adhesion of cationic components to produce an anionic surfactant.

3.2　Surface Modification

Surface modification of colloids and nanostructures through covalent bonds or physical adsorption have been widely considered to enhance their stability,[83] functionality and responsiveness,[84] and to advance their utilization in catalysis,[85] and energy storage applications.[86]. The following sections describe the prospect of polymeric grafts, particularly (i) poly(ethylene glycol) (PEG), and (ii) Poly(glycidyl methacrylate) (PGMA) brushes:

3.2.1　Poly(ethylene glycol) (PEGylation)

Poly(ethylene glycol) is a hydrophilic polymer that can be covalently,[87,88] and physically grafted onto surfaces,[89] or suspended in solution for colloidal stabilization.[90,91]Highly dense PEG brushes on surfaces provide steric barrier against agglomeration and act as a scaffold for structural water to inhibit other molecular interaction with the underlying surface.[92] In this study, covalent attachment of PEG was achieved by producing a polymerizable precursor synthesized through a condensation reaction of a PEG oligomer with maleic anhydride.

3.2.2　Poly(glycidyl Methacrylate) (PGMA) Brush

Poly(glycidyl methacrylate) (PGMA) brushes are widely deployed in surface modification as they contain an epoxy group, which is one of the most versatile functional groups and can be crosslinked,[93] or readily converted into functional moieties using simple chemical reactions.[94] For example, Scheme 6 represents a facile mechanism to produce a negatively charged GMA chain with the addition of sulfite salts, which can be tailored to produce positively charged moieties through alternative amine-derivatives.[95]Tethering PGMA brushes onto colloidal or nanoparticle

suspensions can provide steric and electrostatic stabilization, which is desirable in extreme pH and ionic conditions.
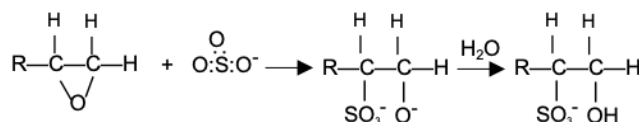
Figure 6 Functionalization of epoxide ring to produce a negatively charged moiety

In this study, the PGMA brush was grafted onto the latex particle that was synthesized by emulsion polymerization. A dispersion seeded polymerization was then initiated, where the polymeric nanoparticle cores, P(VL-co-VA), are allowed to swell with a large amount of GMA monomer, initiator and crosslinker, acting as loci for the polymerization process.[96,97] In the dispersion seeded polymerization, the solvent (water and isopropyl alcohol (IPA), GMA monomer and initiator are miscible whereas the formed PGMA chain has low solvency in the reaction medium. The resulting particle size and surface morphology is influenced by the polymerization conditions; temperature, concentration of GMA monomer/crosslinker, the dropwise monomer feeding rate and agitation.[98] The formation of negatively charges on the PGMA brush was through the addition of sodium sulfite (SS) and sodium bisulfite (SBS) salts in 1:1 weight ratio. The positive functionalization was performed through a two-step process; (i) addition of ethylenediamine (EDA) as a reactive amine,[99] (ii) addition of glycidyltrimethylammonium chloride (GTMAC). The functionalized PGMA yields a polymeric brush with multiple charges contributing to both steric and electrostatic stabilization. In addition, the charged polymeric brush can allow the system to be used for targeted delivery of surfactants to the oil-phase in oil-water mixtures.

34

3.3 CHEMICALS AND MATERIALS

Vinyl laurate (>99.0%), vinyl acetate (>99.0%),sodium persulfate reagent (>98.0%), 3-Allyloxy-2-hydroxy-1-propanesulfonic acid sodium salt solution (40wt% in water), hexadecane (99%), 4,4′-Bis(2-benzoxazolyl) stilbene dye, sodium laurate (99-100%), glycolic acid ethoxylate oleyl ether anionic surfactant (M_n~700), ethylene glycol dimethacrylate (98%), 2,2′-Azobis(2-methylpropionamidine) dihydrochloride (V50) initiator (97%), Triton X-100, ethylenediamine (>99%), glycidyltrimethylammonium chloride (>90%) and divinyl benzene (80%) were purchased from Sigma-Aldrich. Cetyltrimethylamonium Bromide (CTAB) was purchased from AMRESCO. N-Dodecyl-N,N-dimethyl-3-ammonio-1-propanesulfonate (>98.0%) was obtained from Chem-Impex INC. 2-propanol (>99.0%) was purchased from Fisher Chemicals. Maleic Anhydride (>99.0%) and polyoxyethylene(-23)-lauryl-ether were obtained from Sigma-Aldrich. Glycidyl Methacrylate (GMA) (>95.0%) and Sodium Dodecyl Sulfate (SDS) were purchased from TCI chemicals. Sodium chloride (NaCl), calcium chloride dihydrate ($CaCl_2.2H_2O$), magnesium chloride hexahydrate ($MgCl_2.6H_2O$), sodium sulfate (Na_2SO_4), sodium bicarbonate ($NaHCO_3$), sodium sulfite (Na_2SO_3) and sodium bisulfite ($NaHSO_3$ and $Na_2S_2O_5$) were purchased from Sigma-Aldrich. A regenerated cellulose dialysis tubing with 10K molecular-weight cut-off (MWCO) was purchased from ThermoFisher scientific. All materials were used without further purification.

4. CHAPTER 4 : P(VL-*co*-VA) NANOPARTICLES WITH A PROTECTIVE POLY(ETHYLENE GLYCOL) (PEG) SHELL

4.1 EXPERIMENTAL PROCEDURE

4.1.1 Preparation of Polymerizable PEG-Based Shell

The synthesis of the polymerizable polyethylene glycol (PPEG) shell precursor is illustrated in Scheme 1. The molar ratio of maleic anhydride and polyoxyethylene-(23)-lauryl ether was 1:1 and the reagents were mixed at 150ºC for 2 hours followed by 130ºC for 8 hours under continuous nitrogen gas purge and stirring.

4.1.2 Nanoparticle Synthesis: Emulsion Polymerization of P(VL-co-VA)

In a typical synthesis, the poly(vinyl laurate-co-vinyl acetate) P(VL-co-VA) nanoparticles were synthesized through a free-radical emulsion copolymerization of vinyl-laurate and vinyl acetate in 3:1 molar ratio. 0.08 g of N-dodecyl-N,N-dimethyl-3-ammonio-1-propanesulfonate zwitterionic surfactant, 0.4 g of allyloxy-2-hydroxy-1-propanesulfonic acid sodium salt solution comonomer, 0.6 mL of 2-propanol, 0.04g of sodium bicarbonate (NaHCO$_3$) and 0.2g of PPEG were added in 11 ml deionized water and mixed thoroughly. 0.57 g of vinyl-laurate and 0.072 g of vinyl-acetate were added to the above solution under vigorous stirring to form an emulsion. 0.02 g of sodium persulfate was then added, and the emulsion was heated to 60ºC and polymerized overnight. The obtained nanoparticles were purified via dialysis (10K MWCO) for seven days with frequent water replacement.

4.1.3 Characterization of the PEG-Coated P(VL-co-VA) Nanoparticles

The nanoparticle size and zeta potential were determined via dynamic light scattering (DLS) using a Zeta Nanosizer (Malven Instruments, UK). The size

measurement was further confirmed through Scanning Electron Microscopy (SEM) and Transmission Electron Microscopy (TEM).

4.1.4   Alkaline Hydrolysis Accelerated Test

A relatively slow hydrolysis of the ester side chain at neutral or weekly basic pHs is preferred for deep reservoir surfactant delivery. An accelerated alkaline hydrolysis test of the P(VL-co-VA) NPs was used in 0.1M sodium hydroxide (NaOH) in both deionized water and salinity water to shorten the release time. The saline solution composition is illustrated in Table 1.[100]

Table 1 Salt composition to formulate the seawater mixture used in the accelerated hydrolysis.[100]

Salt	NaCl	$CaCl_2.2H_2O$	$MgCl_2.6H_2O$	Na_2SO_4	$NaHCO_3$
Concentration (g/L)	41.04	2.385	17.64	6.343	0.165

To study the effect of temperature on the hydrolysis rate, the alkaline mixture was mixed with the nanoparticle sample in 1:1 weight ratio and stirred at 320 rpm at 80°C and 25 °C. Periodic aliquots were collected from the nanoparticle dispersions at pre-determined intervals after the addition of 0.1M NaOH and titrated with 0.01M hydrochloric acid (HCl). The hydrolysis kinetics were estimated using Equation 5:

$$Hydrolyzed\ Fraction = \frac{mol_{NaOHi} - mol_{HCl\ added} - mol_{-COOH\ (surf)}}{mol_{NaOHi}} \qquad (5)$$

where mol_{NaOHi} is the initial number of moles of sodium hydroxide in the medium, $mol_{HCl\ added}$ is the number of moles of hydrochloric acid added during the titration

to neutralize the solution, and $mol_{-COOH\ (surf)}$ is the number of moles of the carboxylic acid contribution from the PEG shell.

4.1.5 Conductivity Measurements

Conductivity measurements were used to estimate the CMC for the released surfactant and the concentration of surfactant released. The conductivity of the hydrolyzing mixture was benchmarked to the profile of sodium laurate (SL) surfactant, which represents the surfactant produced after hydrolysis. After titrating the hydrolyzing mixture with HCl, sodium chloride (NaCl) salt is formed and has prominent effect on the measured conductivities. Hence, conductivity measurements were collected using EXTECH meter in deionized water and in 0.2% sodium chloride (NaCl) to simulate a similar salt condition formed in the hydrolyzing mixtures. The critical micelle concentration (CMC) was calculated as it provides a significant understanding on the degree of aggregation of amphiphilic surfactant molecules. The conductivity values for hydrolyzing mixtures were measured and correlated to sodium laurate in similar salt conditions.

4.1.6 CMC calculation.

The CMC is an inherent characteristic property of surfactants that is critical to determine the threshold concentration below which optimal surfactant efficacy is achieved. CMC was determined using the intersection of conductivity profiles above and below the critical value.[101]

4.1.7 Contact Angle Measurements

The surfactant ability to alter a substrate wettability was investigated using static contact angle measurements. 0.5g of calcite pellets (13mm in diameter) were

prepared and submerged in model oil under vacuum to generate a carboxyl-functionalized oil-wet surface. Model oil was prepared by mixing 0.01M stearic acid with 50 ml hexadecane at 50ºC overnight.[34]A drop of the unhydrolyzed and hydrolyzed nanoparticle mixture was placed on the substrate and contact angle measurements were collected over time and compared to neat-sodium laurate surfactant in DI water (Figure 5.a-b) and saline water (Figure 5.c-d).

4.1.8   Laser Confocal Scanning Microscopy (LCSM)

Confocal microscopy images were conducted using a Zeiss LSM 710 confocal laser scanning microscope with a Plan-Apochromat ×25, 1.40 water-immersion objective. Emulsions were prepared by vortexing equivolumetric amounts of the nanoparticles with; (i) model oil and (ii) auto-fluorescent crude oil. 4mg of 4,4′-Bis(2-benzoxazolyl) stilbene fluorescent dye was added to the model oil to allow imaging by confocal miscroscopy. To conduct the confocal experiments, few milliliter aliquots of the emulsion were placed between two coverslips on the microscope for imaging.

4.1.9   Dynamic Foam Assessment

Dynamic foamability was evaluated using KRUSS Dynamic Foam Analyzer (DFA100) that detects the foaming height and stability over time as well as capturing the foam structure. 50ml of the respective surfactant and control solutions were placed in the glass column and nitrogen bubbling was initiated at 0.3L/min for 20 seconds while recording the foam height and structure overtime.

4.1.10 Interfacial Tension Measurements (IFT)

Interfacial tension measurement between the nanoparticle suspension and different types of oil (hexadecane, model oil and crude oil) were performed using a KRUSS Spinning Drop Tensiometer (SDT). The heavy phase (DI water, seawater or nanoparticle suspensions at different hydrolysis stages) was placed in the capillary tube and the light phase of the respective oil type were loaded on either the white cap for automatic drop launch or loaded manually into the capillary tube using a syringe for solutions of high IFT. The measurements were conducted under 8000 rpm speed and the IFT was calculated by fitting the Laplace equation to the drop shape.

4.2 RESULTS AND DISCUSSION

4.2.1 Nanoparticle Characterization.

The successful formation of the unsaturated PPEG was determined using Fourier-Transform-Infrared-Spectroscopy (FTIR) transmission and compared with the reagents' spectra as depicted in Figure 7. The spectrum in Figure 1.a for the synthesized PPEG confirm the formation of carbonyl (C=O) vibration at 1715 cm^{-1} and the ether (C-O-C) stretch at 1102 cm^{-1}. The peak at 1780 cm^{-1}contributing to the asymmetric stretch of C=O disappear after the reaction, confirming the conversion of maleic anhydride.[102]
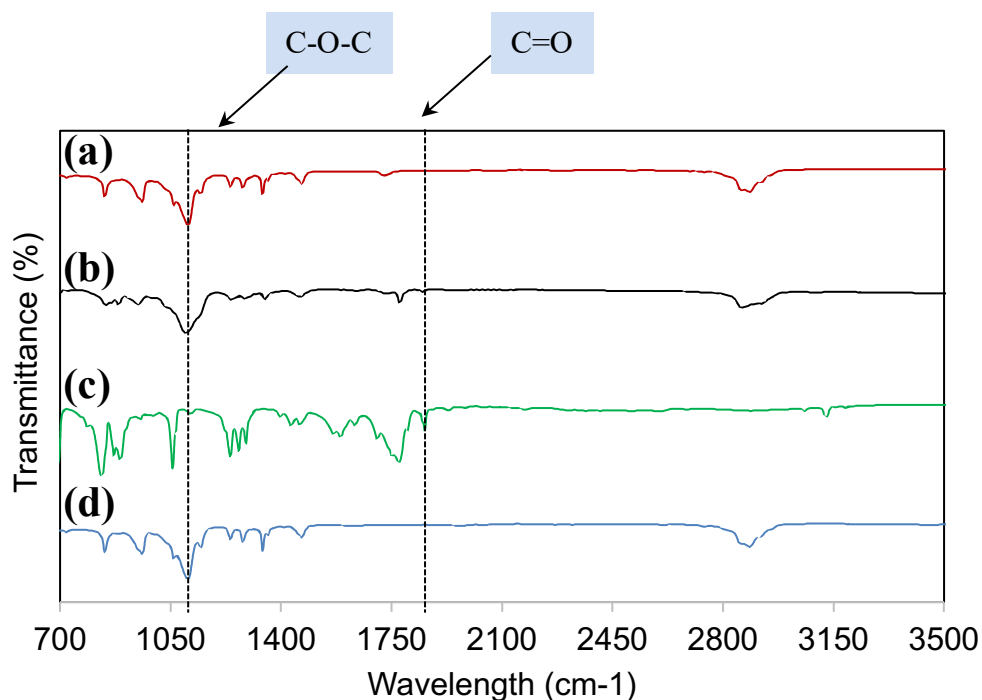
Figure 7 Transmission Fourier-Transform Infrared Spectra for the PEG-based shell. (a) Synthesized polymerizable maleic anhydride/ polyoxyethylene-(23)-lauryl ether in 1:1 mole ratio through a polycondensation reaction , (b) mixture of maleic anhydride and polyoxyethylene-(23)-lauryl ether (1:1) at ambient conditions, (c) maleic anhydride, (d) polyoxyethylene-(23)-lauryl ether.

The PPEG was then copolymerized with the vinyl monomers (vinyl laurate/vinyl acetate) to stabilize the hydrophobic latex core with dual-responsive properties to temperature and pH.[103] The process of PEGylation or polymer coating is a widely investigated technique to stabilize colloidal systems in saline mixtures, which enables a diverse range of industrial and biological applications.[88,104] Zhang and co-workers found that ultrahigh colloidal stability is achieved in high ionic strengths and extreme pH conditions, when loading thiolated-DNA on gold nanoparticle (AuNP) in PEG mixtures.[90] The incorporation of the hydrophilic comonomer, allyloxy-2-hydroxy-1-propanesulfonic acid sodium salt solution, can further enhance the stability and the size distribution of the polymeric latex.[105,106] 2.5wt% and 5wt% of monomer concentrations

were evaluated for stability in saline water and size distribution as demonstrated in Figure 8.
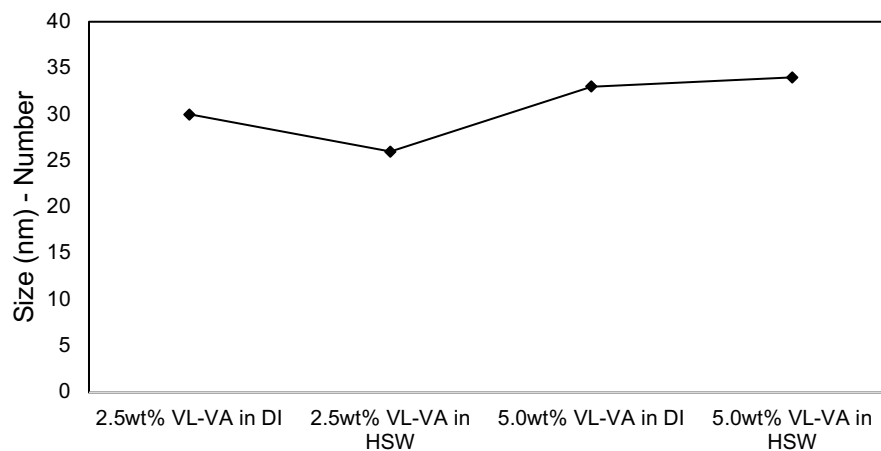
Figure 8 Nanoparticle size measurements for different monomer concentrations in saline and DI water

Since there was no significant change in the nanoparticle at different monomer concentrations, 5wt% monomer concentration was selected and a scaled-up 400ml batch was synthesized and characterized by DLS, TEM and SEM (Figure 9). They all confirmed the formation of spherical P(VL-co-VA) NPs that are 55.0 ± 8 nm in size with zeta potential of -54 mV.

(a)
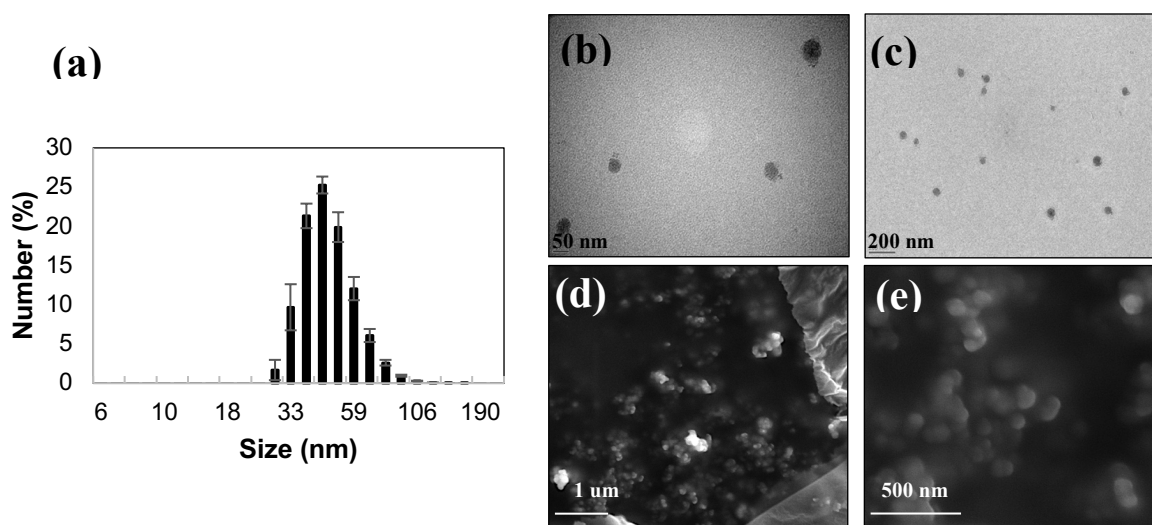
Figure 9 (a) DLS measurement of P(VL-co-VA) NPs (b) and (c) TEM images of PEG-coated, unhydrolyzed, P(VL-co-VA) nanoparticles. Scale bar: 50 nm for (b) and 200 nm for (c). (d) and (e) SEM images of unhydrolyzed, P(VL-co-VA) nanoparticles. Scale bar: 1 μm for (d) and 500 nm for (e).

4.2.2   Hydrolysis Kinetics.

Owing to our interest in the slow release of surfactants in both oil spill remediation as well as enhanced oil recovery, we began by studying the hydrolysis kinetics at different temperatures and salinities. To that end, sodium hydroxide was used for accelerated hydrolysis to evaluate the release at a shorter time. The bare p-(VL-co-VA) NP core exhibits a fast hydrolysis profile in 0.1M NaOH at 80°C (Figure 10), resulting in ~66% hydrolysis after one day. The fast release prompted the need to incorporate a PEG shell to inhibit the accessibility of hydroxyl groups for a more controlled, slow-release profile. The following sections describe the hydrolysis behavior in varying temperatures, and salinity conditions. Although the primary objective was to design a nanoparticle platform with slow-release profile in neutral

reservoir conditions of pH 7.5, an accelerated hydrolysis test allows the evaluation

of the interplay of external stimuli in complex reservoir dynamics. The performance

of the released surfactant was also benchmarked against sodium laurate.
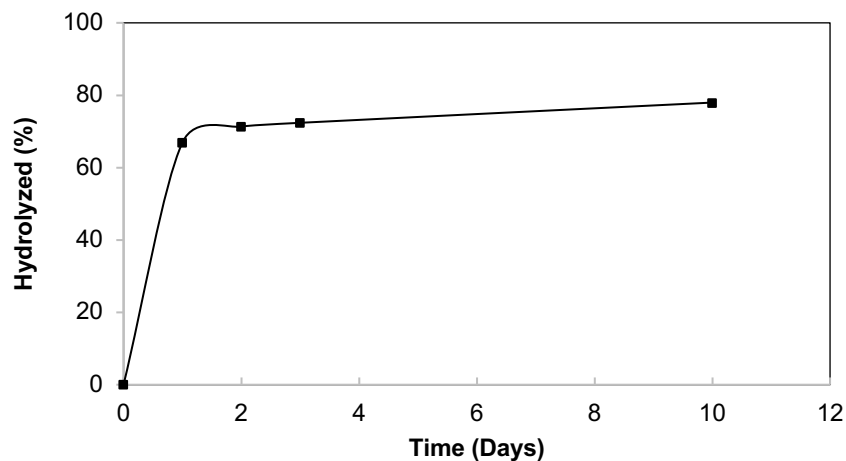
Figure 10 Calculated % of hydrolysis using titration with 0.01M HCl for
bare, un-PEGylated P(VL-co-VA) NP cores with 0.1M NaOH solution.

4.2.2.1 Effect of Temperature.

Alkaline-assisted hydrolysis of the ester side chain of vinyl-laurate using sodium

hydroxide is a convenient approach to produce lauric acid that reacts with sodium ions

to yield the desired surfactant [R-COO⁻Na⁺]. Figure 11 shows the release profile in

0.1M sodium hydroxide at and 25°C and 80°C, respectively.
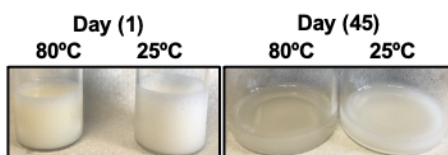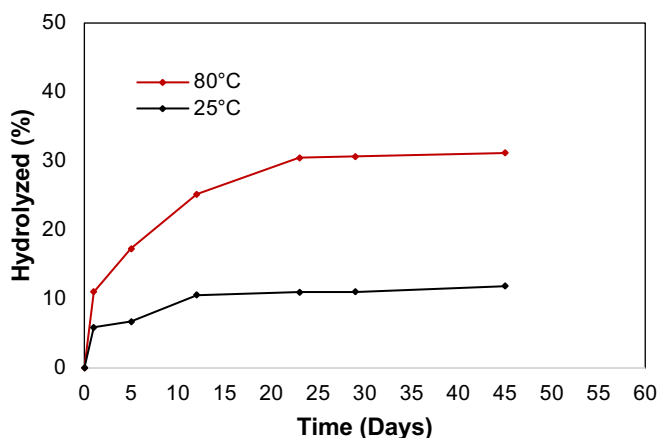
Figure 11 Calculated hydrolysis (%) of P(VL-co-VA) NPs in deionized water with buffer concentration of 0.1M NaOH at 80ºC and 25ºC.

The release profile in alkaline conditions shows a slow release with only 31 and 11% of surfactant release at 80ºC and 25ºC, respectively, within around 45 days followed by a plateau stage with a much slower release rate. This behavior can be explained by the initial consumption of the carboxylic acid product by the basic ions [OH⁻] in solutions, driving the reaction forward. After neutralizing the hydroxyl ions in solution, the produced acid becomes less soluble driving the reaction to equilibrium. Although the initial abrupt increase in hydrolysis is observed at high and low temperatures, the temperature-dependence of the hydrolysis rate is confirmed at longer time intervals. Several parameters can influence the slow hydrolysis rate. In base-catalyzed hydrolysis, the structural configuration and the chain length of the aliphatic ester groups have prominent effect on the reaction rate.[107] As the chain length increases, such as in vinyl laurate, the reaction rate decreases, which is desirable in applications

where slow-release is favorable. TEM images of the hydrolyzed P(VL-co-VA) NPs presented in Figure 12 further demonstrate low-contrast bright patches that are attributed to the released surfactant molecules. The morphology of the hydrolyzed nanoparticles was partially altered to an extended polymer chain after the hydroxyl group attack on the ester side chain. The TEM images further reveal the presence of nanoparticle clusters that retained the spherical structure as the hydrolysis did not go to completion.
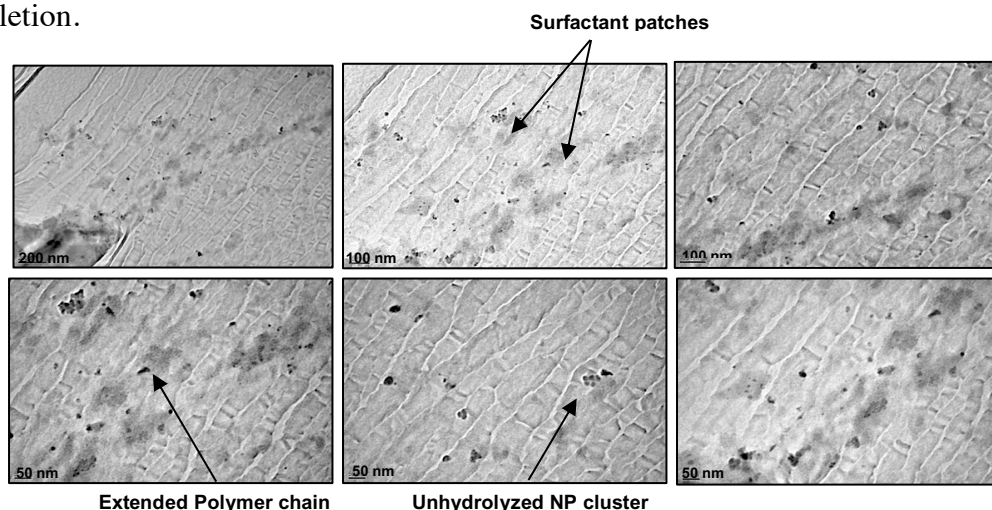
Figure 12 TEM images of hydrolyzed P(VL-co-VA) in deionized water

4.2.2.2 *Effect of Water Salinity.*

To evaluate the effect of salinity on the surfactant delivery, P(VL-co-VA) NPs were suspended in synthetic saline water. [100] Figure 13.a demonstrates the release profile in high salinity water using 0.1M NaOH. Solutions of high ionic strengths trigger a faster release profile in comparison to the hydrolysis in deionized water observed in Figure 11. Hydrolysis in saline water resulted in 76% and 22% of surfactant release after 54 days at 80 and 25 ℃, respectively.
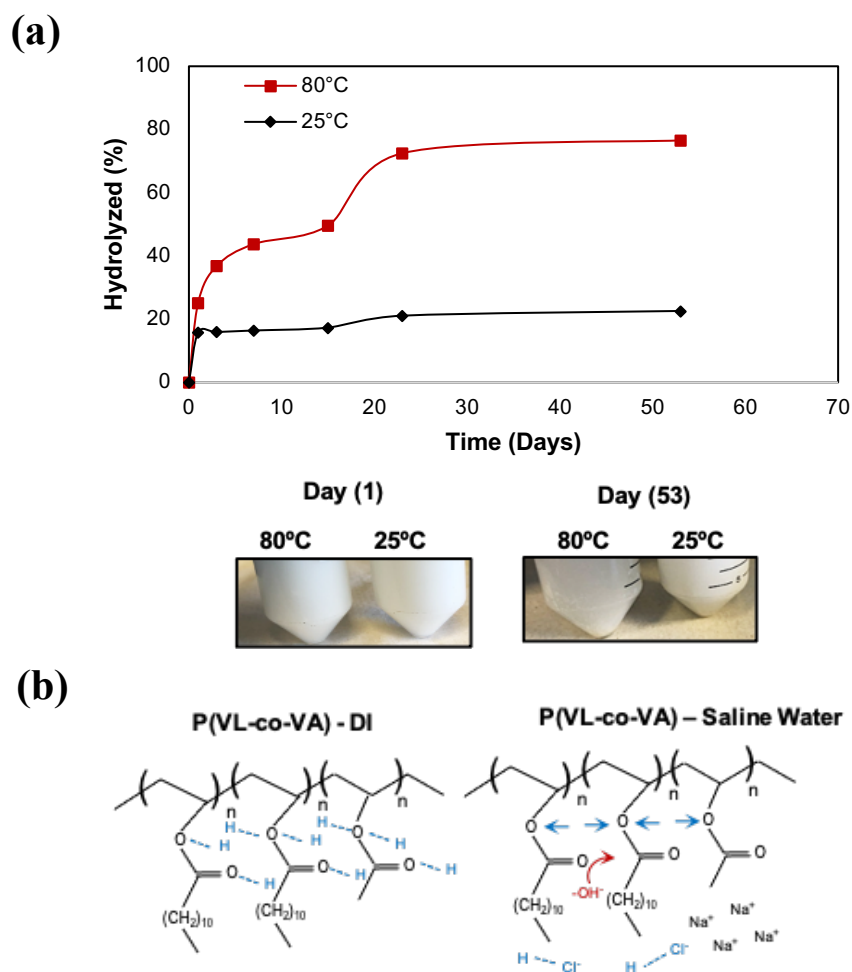
Figure 13 (a) Release profile of P(VL-co-VA) NPs in high salinity water in 0.1M NaOH at 80ºC and 25ºC, (b) Effect of Salt-catalyzed hydrolysis and disruption of H-bonding

Salt-catalyzed hydrolysis, particularly metal chlorides (e.g NaCl), has been extensively studied in enhancing the generation of acidic products, most notably in the depolymerization of cellulose to generate acid-derived precursors (e.g. levulinic acid) for the production of biofuels.[108] The formation of water-anion hydrogen-bonded networks in highly concentrated chloride salt solutions plays a significant role in disrupting the ester-water coordinated clusters and allows hydroxyl (-OH$^-$) accessibility to the carbonyl groups as depicted in Figure 13.b.[109,110] Furthermore, in low salt concentrations, the hydrophilic components in PEG form strong hydrogen

bonding with the surrounding water molecules, which allows for a uniformly dispersed protective shell.[111] In salt solutions, cations are immobilized in PEG due to the ion complexation with crown ethers disrupting the structured shell,[112] which allows for more accessible hydroxyl ($-OH^-$) nucleophilic attack and which results in faster hydrolysis. Furthermore, salts dissociate into their constituent cations/anions and alter the acidity/basicity of the solution depending on their conjugate acids and bases.[113] Additionally, molecular interactions of metal ions with carboxylic acids have been vastly studied in wastewater treatments as absorbents.[114] Most notably, carboxylates ($R-COO^-$) tend to exhibit high-affinity in forming ion-pairs with monovalent cations in solution.[115,116]At the hydrolyzing pH conditions (~13), the (-COOH) groups in lauric acid are deprotonated and metal ion uptake occurs driving the hydrolysis reaction forward.

4.2.2.3 Effect of pH

To assess the kinetics profile in strongly basic solutions, a 2 M NaOH sodium hydroxide hydrolyzing mixture was prepared in DI and mixed with the P(VL-co-VA) NPs in 1:1 weight ratio yielding a 1M NaOH alkaline concentration. The percent hydrolysis was calculated and shown in Figure 14.
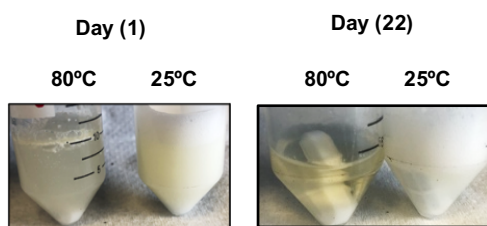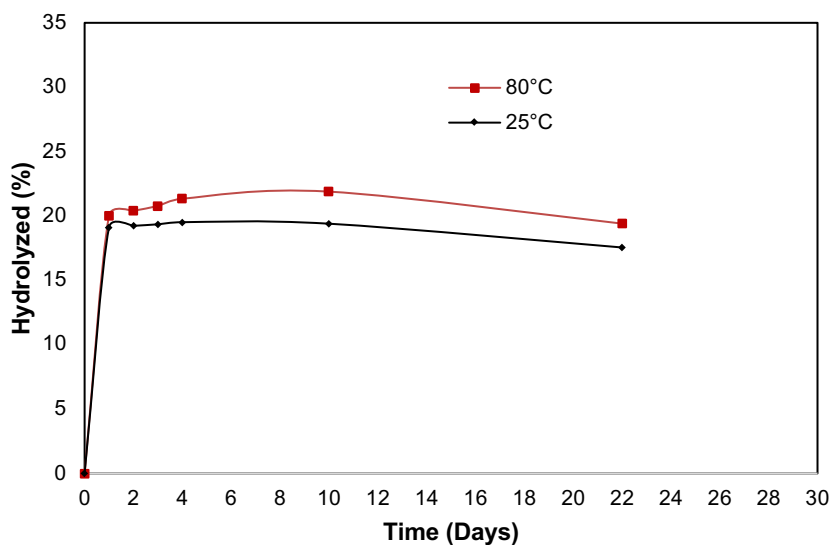
Figure 14 Calculated hydrolysis (%) of P(VL-co-VA) NPs in deionized water with buffer concentration of 1M NaOH at 80ºC and 25ºC.

It can be noted from the hydrolysis comparison between the 1M and 0.1M NaOH, that the periodic titration calculation fails to approximate the release in highly concentrated alkaline mixtures. The nanoparticle mixture could be fully hydrolyzed by a very small amount of the 1 M NaOH mixture leaving excess hydroxyl ions that require larger volumes of HCl to be neutralized, which underestimate the hydrolysis percentage as per Equation 5. Conductivity measurements were applied as an alternative method in the surfactant release assessment for the hydrolyzing mixture in 1 M NaOH by correlation to sodium laurate (SL) commercial surfactant. After titrating the hydrolyzing mixture with

HCl, sodium chloride (NaCl) salt is formed and has prominent effect on the measured conductivities. Hence, conductivity measurements were collected in deionized water and in 0.2% sodium chloride (NaCl) to simulate a similar salt condition formed in the hydrolyzing mixtures (Figure 15). The measured CMC values for sodium laurate in DI and 0.2% NaCl were 0.026 M and 0.0166 M, respectively, as inferred from Figure 15. The estimated value for the CMC in DI water agrees with the values reported by Campbell and co-workers.[93] The conductivity values for hydrolyzing mixtures were measured and correlated to sodium laurate in similar salt conditions to obtain an estimate of the hydrolysis profile in Figure 16.
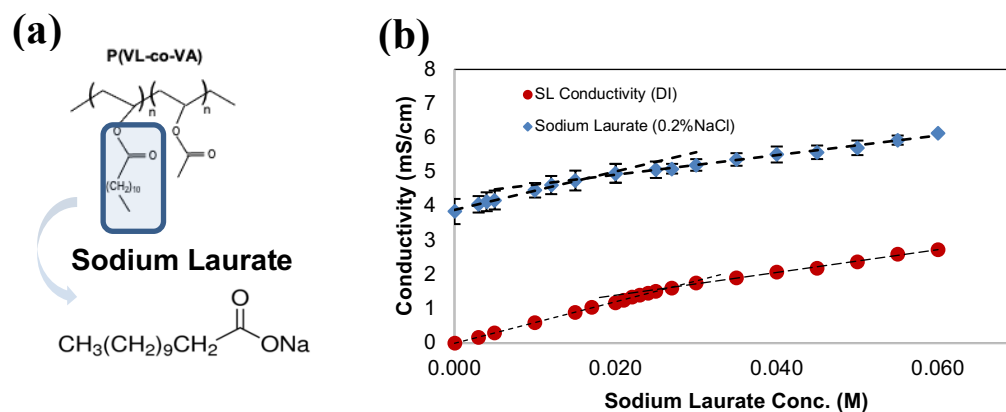
Figure 15 (a) Schematic representation of the produced surfactant, (b) Sodium laurate conductivity measurements in deionized water and 0.2% sodium chloride (NaCl) concentration.
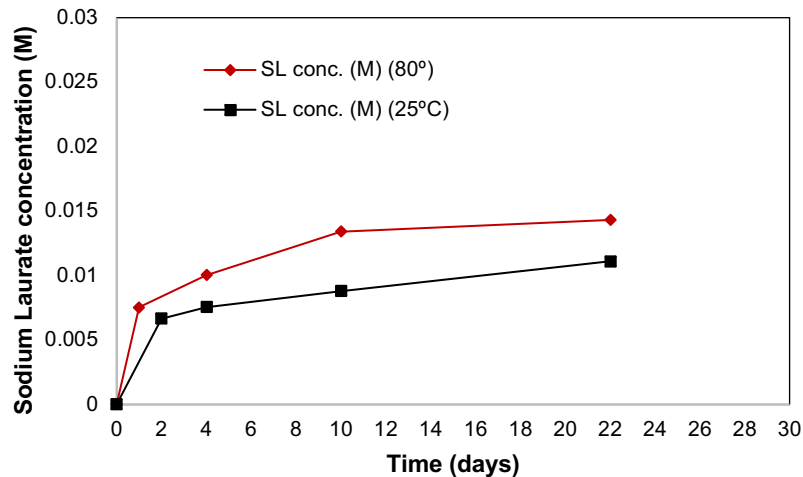
Figure 16 Estimated sodium laurate concentration released after hydrolysis in 1M NaOH at 80ºC and 25ºC using conductivity measurements.

4.2.3   Wettability Alteration: Static Contact Angle Assessment

A sessile drop contact angle analysis was conducted on an oil-wet calcite substrate at ambient conditions to investigate the hydrolyzed mixture ability in altering the wetting state. To achieve maximum surfactancy in deionized water, a highly concentrated 1M NaOH buffer was utilized to hydrolyze the NP mixture.

4.2.3.1   Effect of Nanoparticle Concentration

To determine the optimum nanoparticle concentration required to alter wettability, 10, 100 and 1000 ppm of the nanoparticle mixture were suspended in DI and contact angle measurements were collected as depicted in Figure 17. 1000 ppm P(VL-co-VA) NPs suspension, below the CMC, was selected to assess the surfactant efficacy in altering the wettability of an oil-wet calcite substrate.
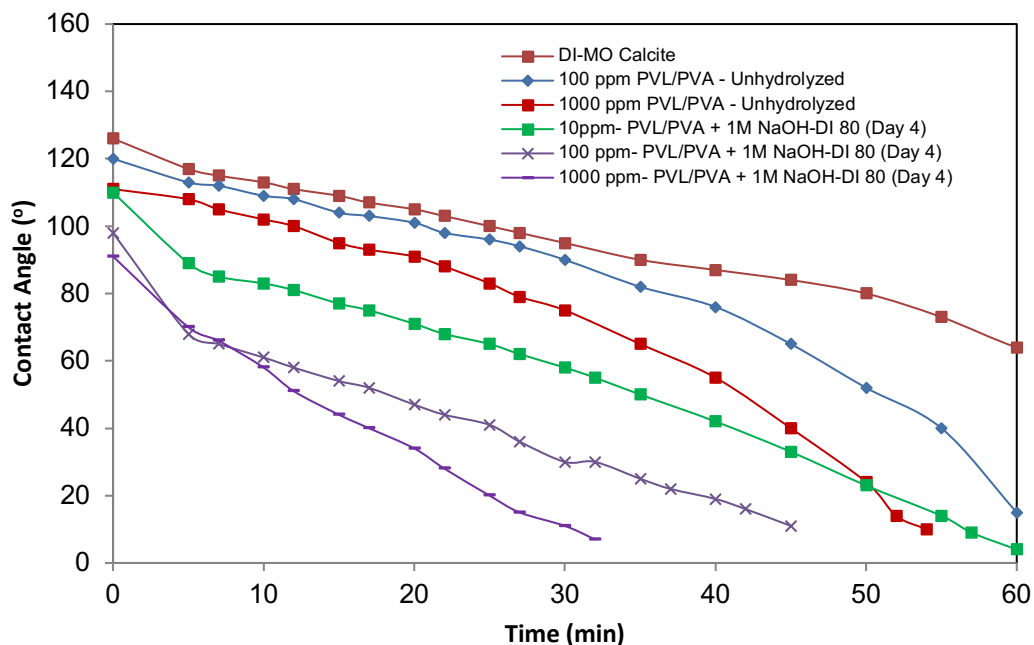
Figure 17 Contact angle measurements of P(VL-co-VA) NPs suspended in DI water at varying concentrations and hydrolysis conditions.

Deionized water on oil wet calcite shows the highest IFT with a contact angle of 118°. A slow gradual decrease of the contact angle observed with time is due to the spontaneous imbibition within the calcite pores. When a sodium laurate surfactant is used a lower initial contact angle of 100° is seen with a longer period required to alter the wetting state. The P(VL-co-VA) unhydrolyzed NP system exhibits a similar onset contact angle (113°) compared to deionized water but with an accelerated drop that crosses with the profile of sodium laurate after 25 minutes. The unhydrolyzed P(VL-co-VA) NPs trend can be explained by the surfactancy on the nanoparticle surface and the PEG surrounding layer. The hydrolyzed P(VL-co-VA) NPs collected at different time intervals demonstrate the maximum spreading tendency on the hydrophobic surface compared to the previous solutions combining the effect of NPs and released surfactant. The relatively faster hydrolysis profile in salt conditions discussed earlier is further

confirmed with the contact angle measurements as demonstrated in Figures 18.c and d. The unhydrolyzed P(VL-co-VA) NPs in high salinity water revealed a better performance in altering the wetting state compared to the commercial sodium laurate surfactant at similar ionic strengths. The hydrolyzed P(VL-co-VA) NPs in salt solutions demonstrate the maximum efficacy of the system in altering the wetting state from 75º to complete spreading in only 17 minutes even at lower concentrations.

(a)

(b)

30 mins

(d)

30 mins
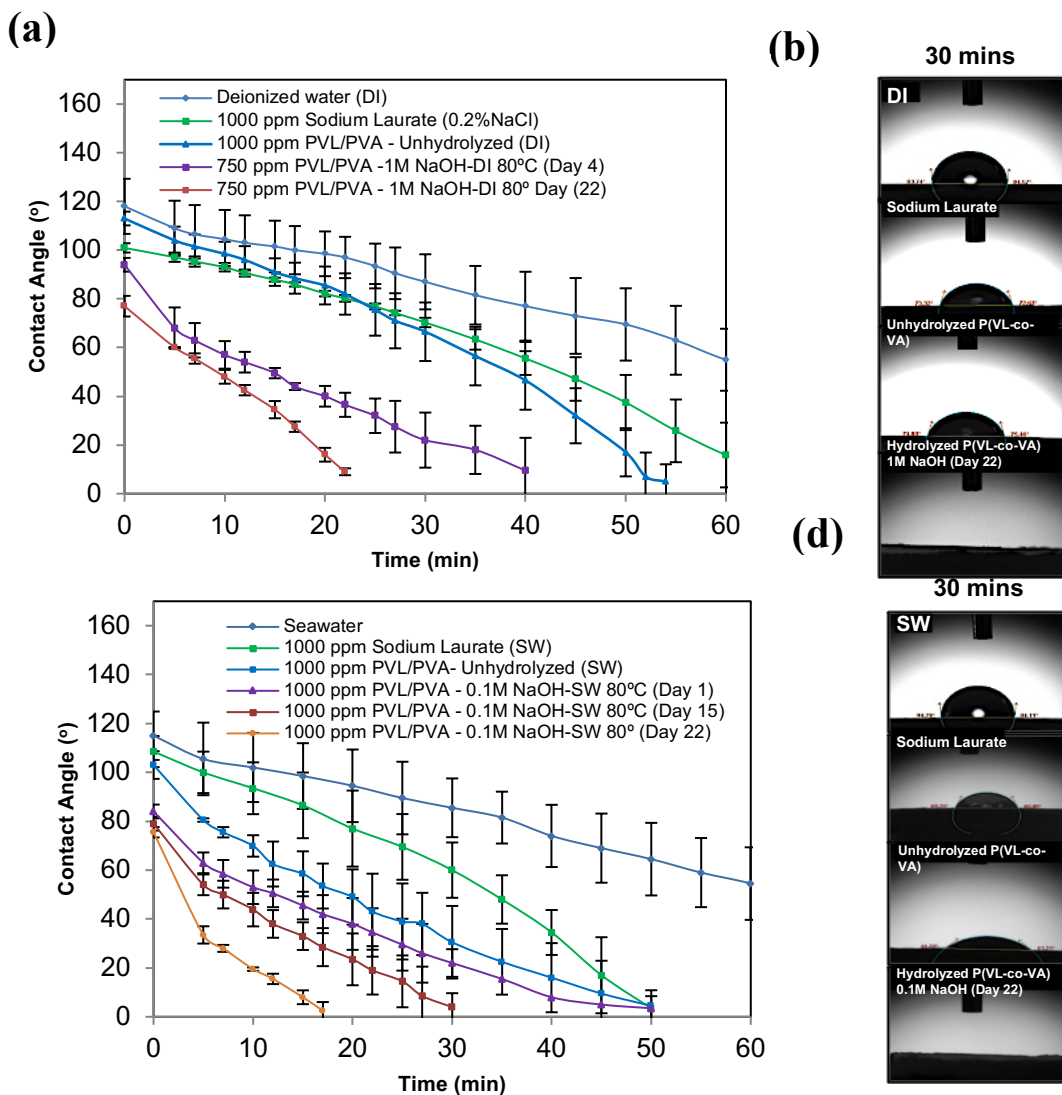
Figure 18 Contact angle profile and images on a calcite pellet saturated with model oil (0.01M stearic acid in hexadecane). Measurements were conducted: (a) & (b) in deionized water and (c) & (d) in high salinity water. Data was collected for the water medium, 1000 ppm sodium laurate surfactant, 1000 ppm unhydrolyzed P(VL-co-VA) nanoparticles and the titrated hydrolyzed P(VL-co-VA) in a respective alkaline mixture at 80ºC.

4.2.4   Emulsification: Laser Confocal Scanning Microscopy (LCSM).

Emulsions are of great practical interest in many industrial and scientific applications.[117,118] To evaluate the potential use of P(VL-co-VA) NPs in emulsifying

two immiscible phases, suspensions of the hydrolyzed and unhydrolyzed NPs were mixed with model oil (Figure 19) and crude oil (Figure 20) samples. LCSM micrographs for model oil illustrated in Figure 19.a and b and DI water in the absence of surfactants show formation of thermodynamically unstable globules that undergo Oswald ripening resulting in larger droplet sizes. The hydrolyzed nanoparticles in 1M NaOH captured in Figure 19.c, confirm the ability of the released surfactant to stabilize microemulsions with improved solubilization and entrapment of both hydrophilic and lipophilic phases. Similar results were obtained for crude oil-water mixtures (Figure 20). Figures 20.b and 20.c emphasize the difference in behavior between the *unhydrolyzed* and *hydrolyzed* p-(VL-co-VA) NPs. As before, the presence of surfactant from the addition of the already *hydrolyzed* NPs to the oil-water mixture stabilizes the emulsion and produces smaller droplets.
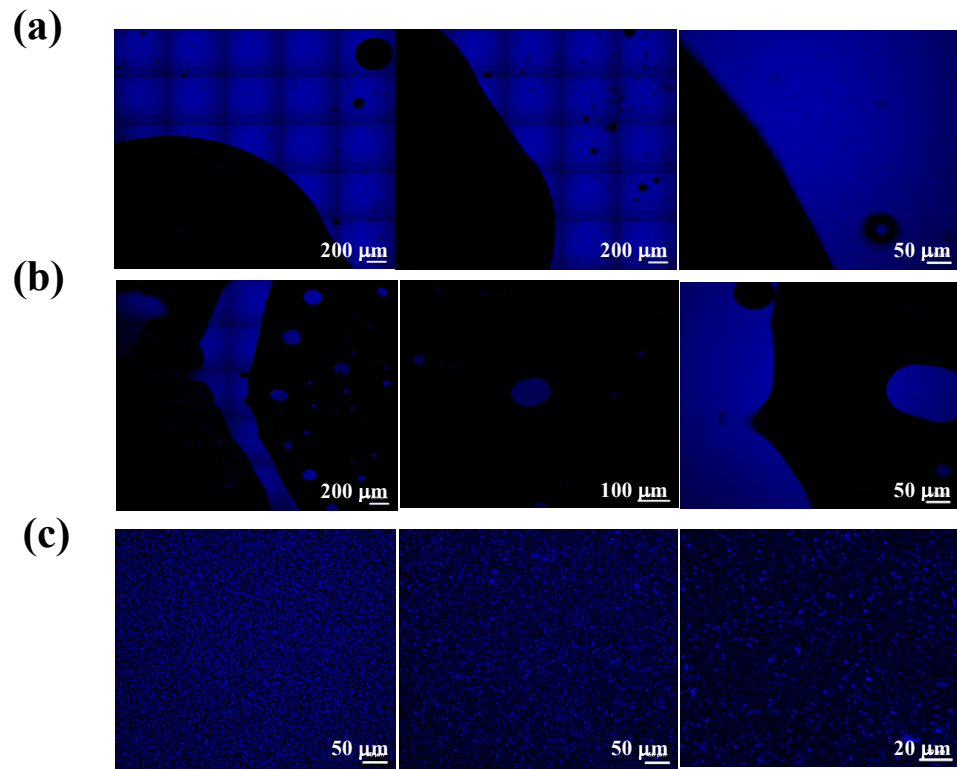
Figure 19 Confocal Micrographs of (a) model oil in deionized water, (b) unhydrolyzed P(VL-co-VA) NPs in model/DI, (c) hydrolyzed P(VL-co-VA) NPs in model oil/DI.
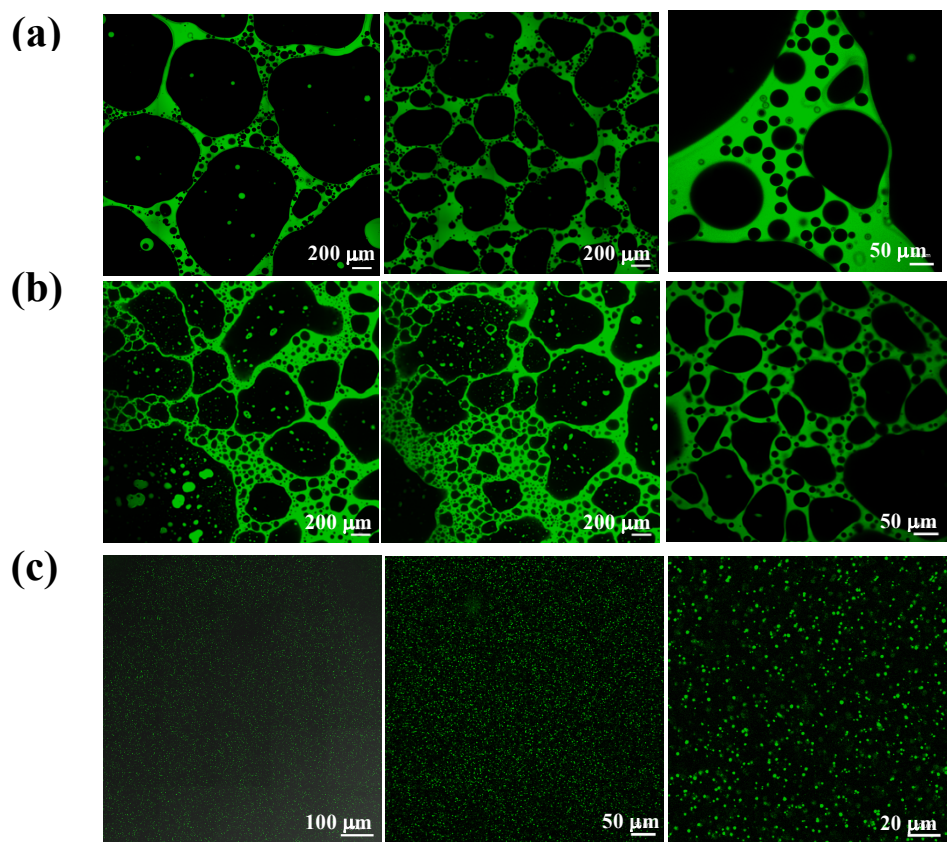
Figure 20 Confocal Micrographs of (a) crude oil in deionized water, (b) unhydrolyzed P(VL-co-VA) NPs in Crude oil/DI, (c) hydrolyzed P(VL-co-VA) NPs in Crude oil/DI.

4.2.5 Foamability: Dynamic Foam Analyzer

The foamability of aqueous solutions is of great practical interest in EOR applications. Typical gas injection, through CO_2 or N_2, yields low volumetric sweep due to the low density of gases compared to crude oil or water in the reservoir.[119] The unfavorable mobility ratio of gas flooding resulting in gas channeling, early gas-

breakthrough, viscous fingering and gravity segregation, can be addressed by foaming of the injected gases (Figure 21).[120]
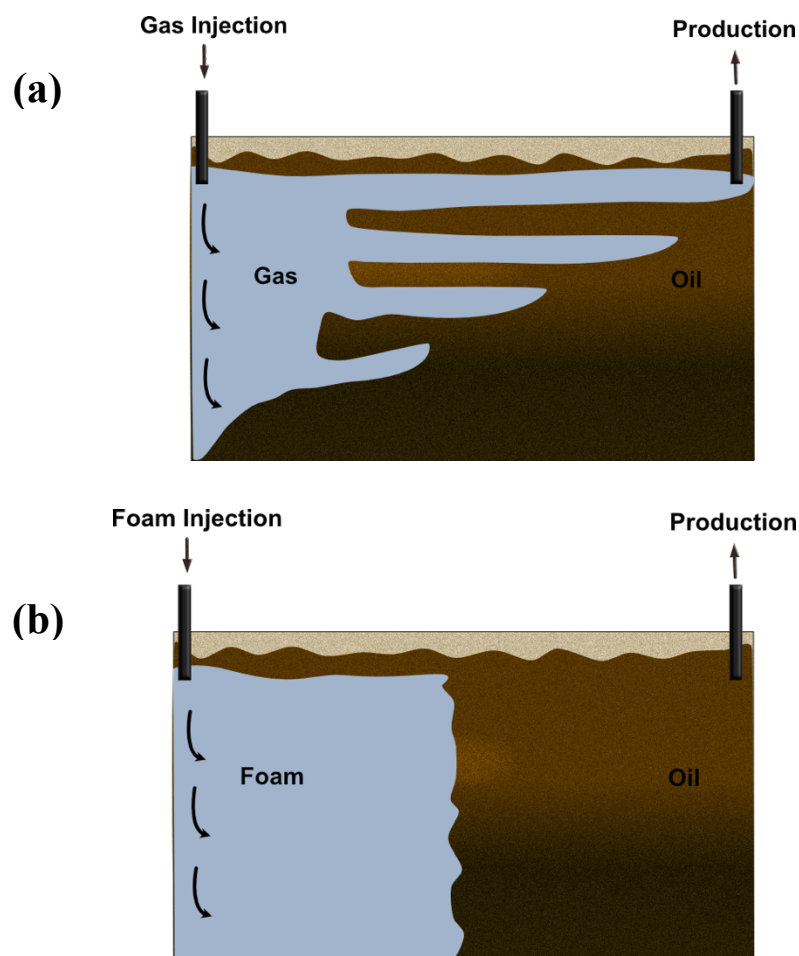
Figure 21 (a) Gas flooding exhibiting channeling, breakthrough, and gravity segregation, (b) foam injection yielding uniform sweep

To assess the foamability of the hydrolysable nanoparticle system, solutions containing 100 ppm hydrolyzed/unhydrolyzed P(VL-co-VA) NPs and sodium laurate surfactant in DI and saline water were bubbled with nitrogen for 20s and the foam height and structure were recorded as depicted in Figures 22 and 23. Significant foam generation is detected in hydrolyzed P(VL-co-VA) NPs solutions in DI water compared to saline water. However, the foam half-life time in the hydrolyzed system

is short (52s in DI and 25s in saline water). The low stability can be attributed to the coalescence and fusion of bubbles after rupturing of the liquid film as detected in the images of the foam structure. The rupturing of the liquid film is controlled by the surface elasticity and the ability of the surfactants to redistribute from the bulk of the film to the interface, which is hindered in low surfactant concentrations.[121] In surfactants containing carboxylic acids, the maximum stability can be achieved at conditions, where pH ~ PK_a. This is due to the fact that only ~50% of the carboxylic acid groups are ionized, prompting the formation of acid-soap H-bonding.[122] In neutral conditions where the pH is higher than the pK_a of lauric acid (~5.3), ionic repulsion is initiated between the anionic surfactant head groups inducing film thinning (Figure 24). At high salt concentrations (Figure 23.a and b), complexation of the negatively-charged head group with cations result in a screening effect yielding a thinner and less stable film. [123]
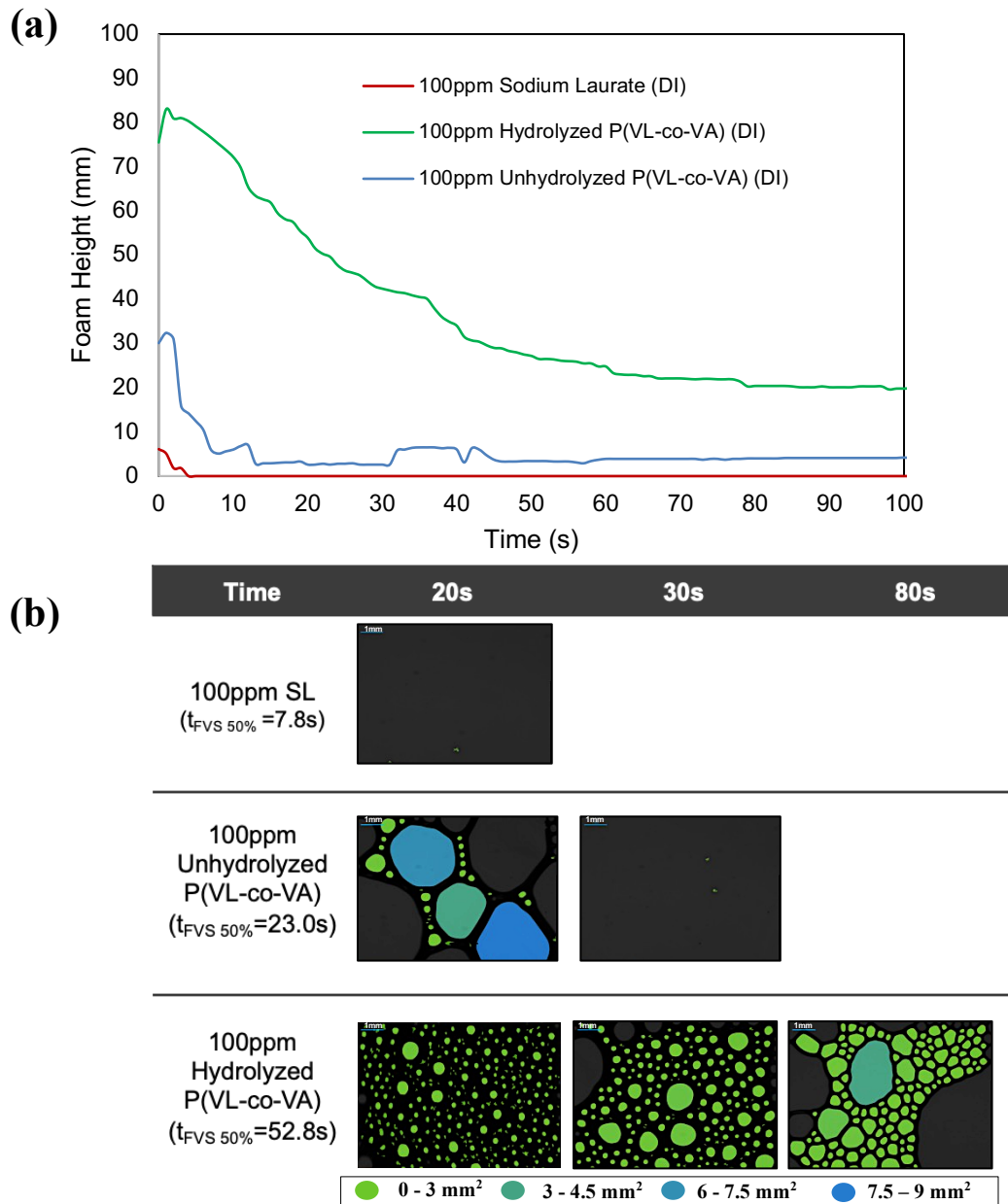
Figure 22 (a) Foam height profiles of 100 ppm solutions of sodium laurate, hydrolyzed P(VL-co-VA) NPs, and unhydrolyzed P(VL-co-VA) NPs in DI, (b) foam structure of surfactant solutions captured after 20, 30 and 80s of foaming. *(The different color overlays in foam structure represent the respective bubble area size range)*
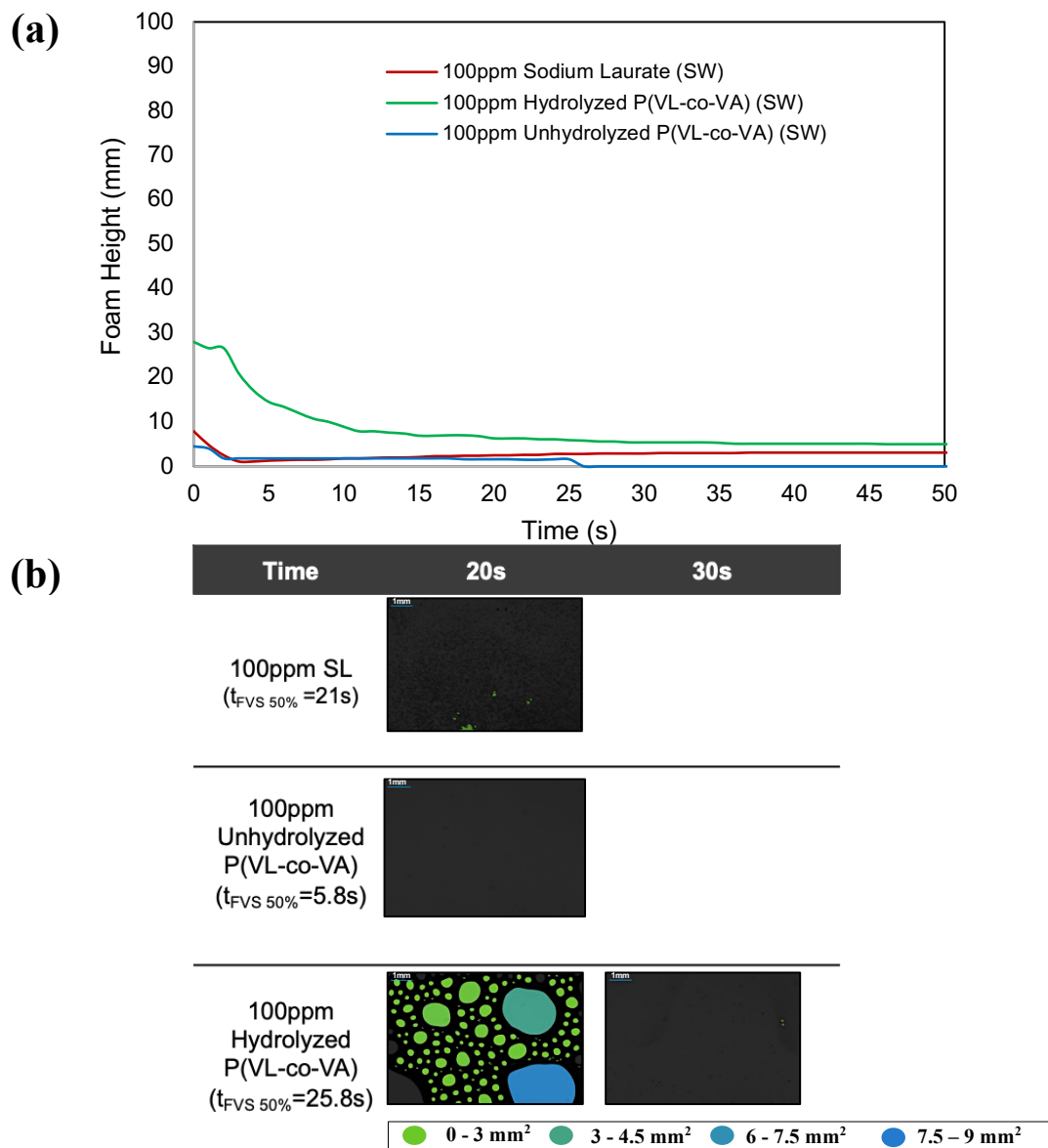
Figure 23 (a) Foam height profiles of 100 ppm solutions of sodium laurate, hydrolyzed P(VL-co-VA) NPs, and unhydrolyzed P(VL-co-VA) NPs in seawater, (b) foam structure of surfactant solutions captured after 20, and 30s of foaming. *(The different color overlays in foam structure represent the respective bubble area size range)*

(a) **(b)**
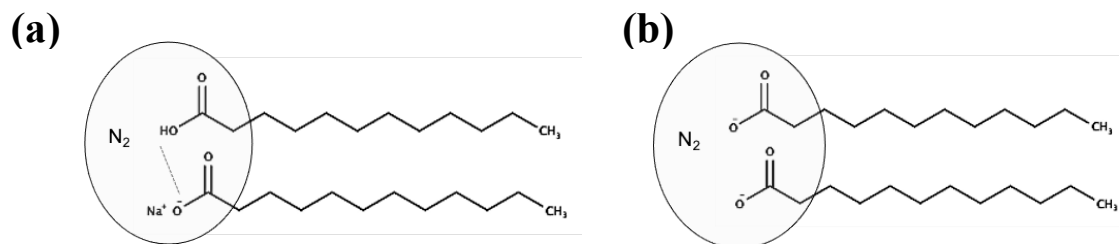
Figure 24 Effect of ionization state of carboxylate group on the film thickness and foam stability, (a) at pH ~ pKa, the presence of protonated and deprotonated states leads to the formation of intermolecular H-bonding, (b) at pH > pKa, the deprotonated state dominates and electrostatic repulsion induces film thinning. Adopted from Stubenruach et al. [122]

4.2.6 Interfacial Tension (IFT) Measurements

IFT measurements of unhydrolyzed / hydrolyzed P(VL-co-VA) NPs suspensions at different hydrolysis intervals and oil (hexadecane in Figure 25, model oil Figure 26, and crude oil Figure 27) were carried out. The IFT for DI water and hexadecane is 36 mN/m and 27 mN/m for DI water and model oil or crude oil. The addition of salts reduces the IFT, which is more prominent in model oil and crude oil (~ 6 mN/m). The recorded IFT values for the oil water mixtures falls within the range of values reported in the literature.[124] To distinguish the effect of 0.2% NaCl present after the titration, a solution of 0.2% NaCl in DI water was prepared and the IFT was ~ 21 mN/m (Figure 27.a). This indicates that the majority of IFT reduction originates from the presence of the neat P(VL-co-VA) NPs, irrespective of the hydrolysis or any salt present. After hydrolysis of the NPs, little to marginal IFT reduction is recorded suggesting that the IFT measurement is less sensitive to the surfactant release compared to other interfacial measurements such as the contact angle measurement. It has been also reported that the IFT change alone is not responsible for a drop in contact angle, and solutions with high IFT still demonstrate a reduction in contact angle.[125]

(a)

(b)
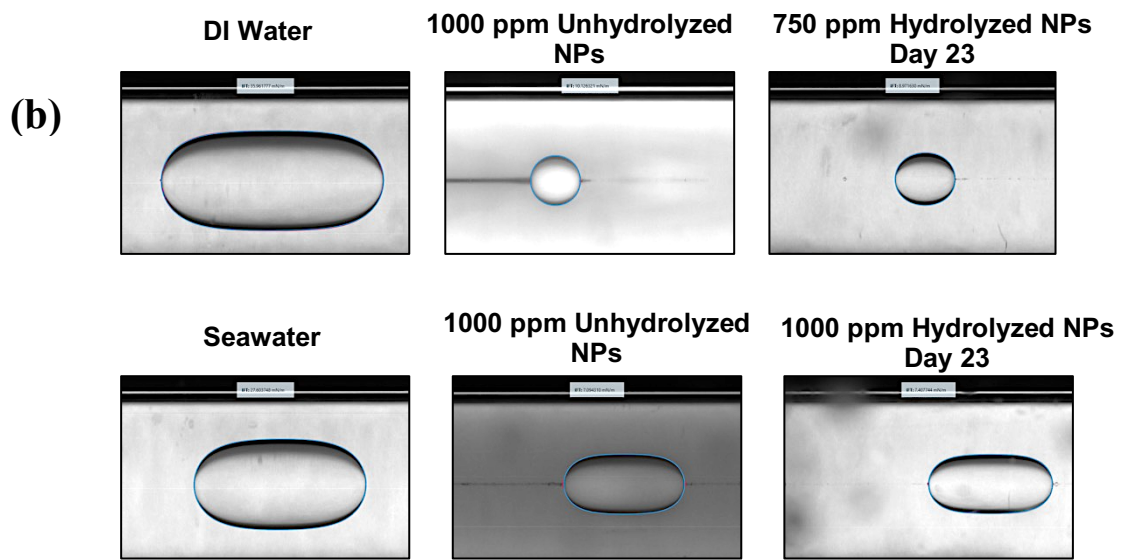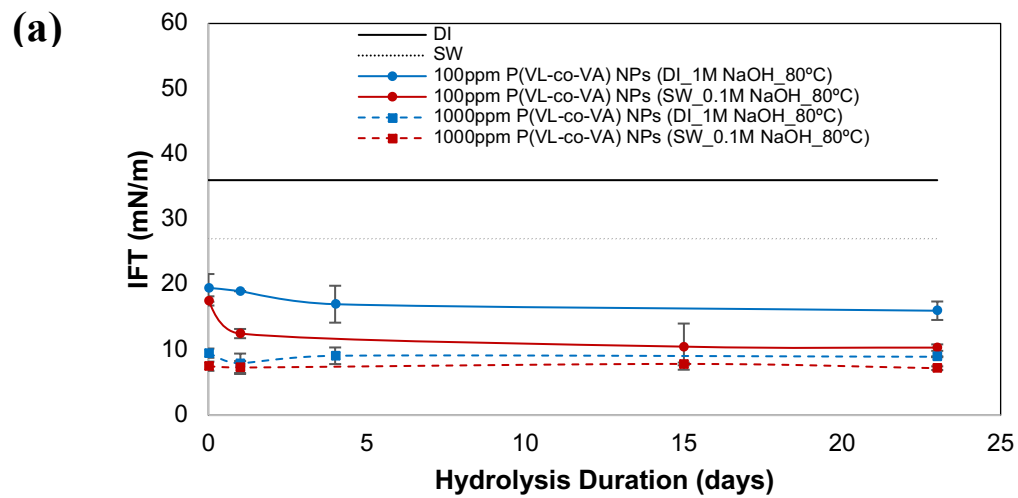
Figure 25 (a) IFT measurements of hexadecane in DI water or seawater at 8000rpm in comparison to the unhydrolyzed and hydrolyzed NPs at different hydrolysis, (b) hexadecane droplet image.

(a)

(b)
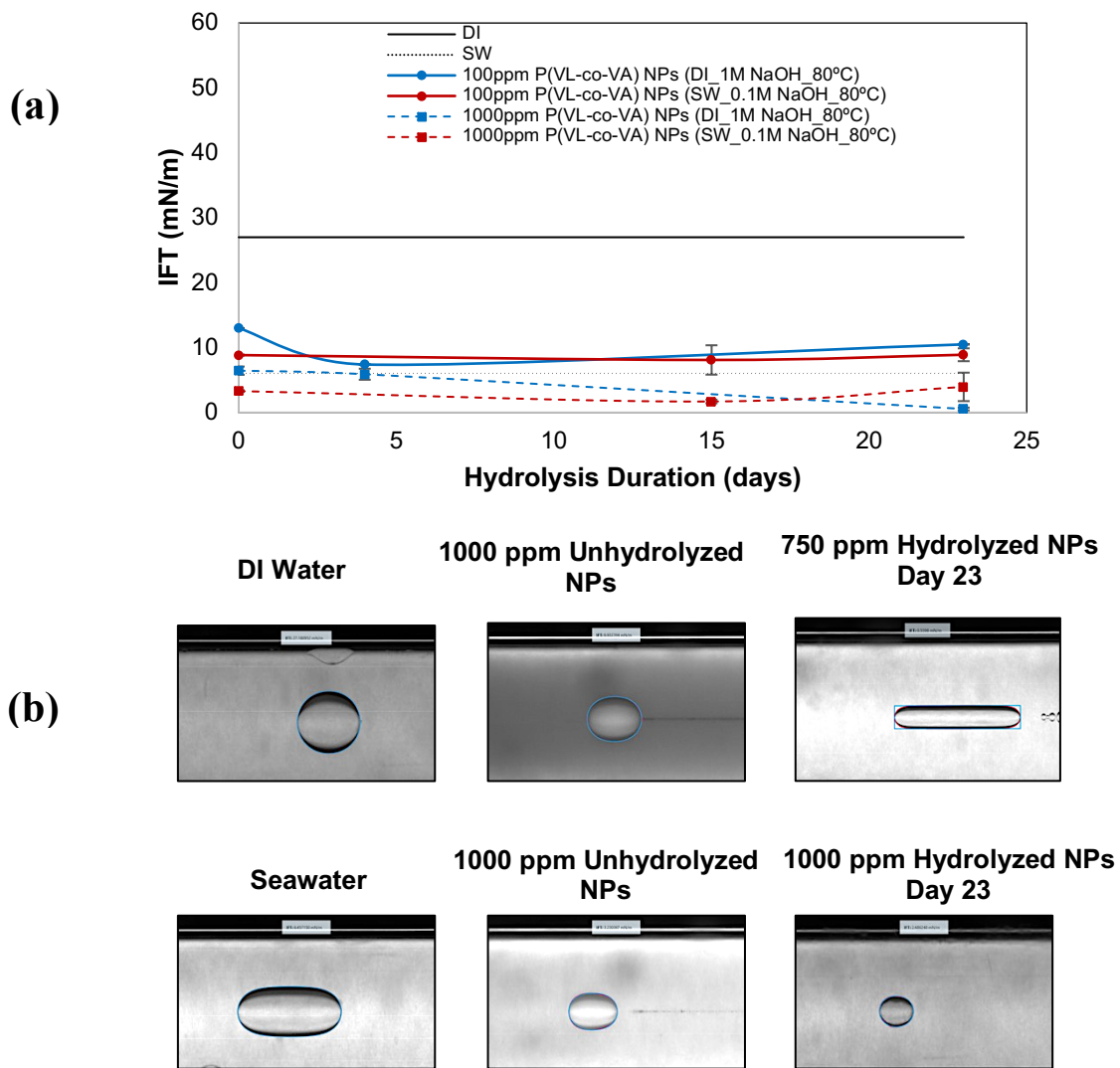
Figure 26 (a) IFT measurements of model oil in DI water or seawater at 8000rpm in comparison to the unhydrolyzed and hydrolyzed NPs at different hydrolysis, (b) model oil droplet image.

(a)

(b)

| DI Water | 1000 ppm Unhydrolyzed NPs | 750 ppm Hydrolyzed NPs Day 23 |
| Seawater | 1000 ppm Unhydrolyzed NPs | 1000 ppm Hydrolyzed NPs Day 23 |
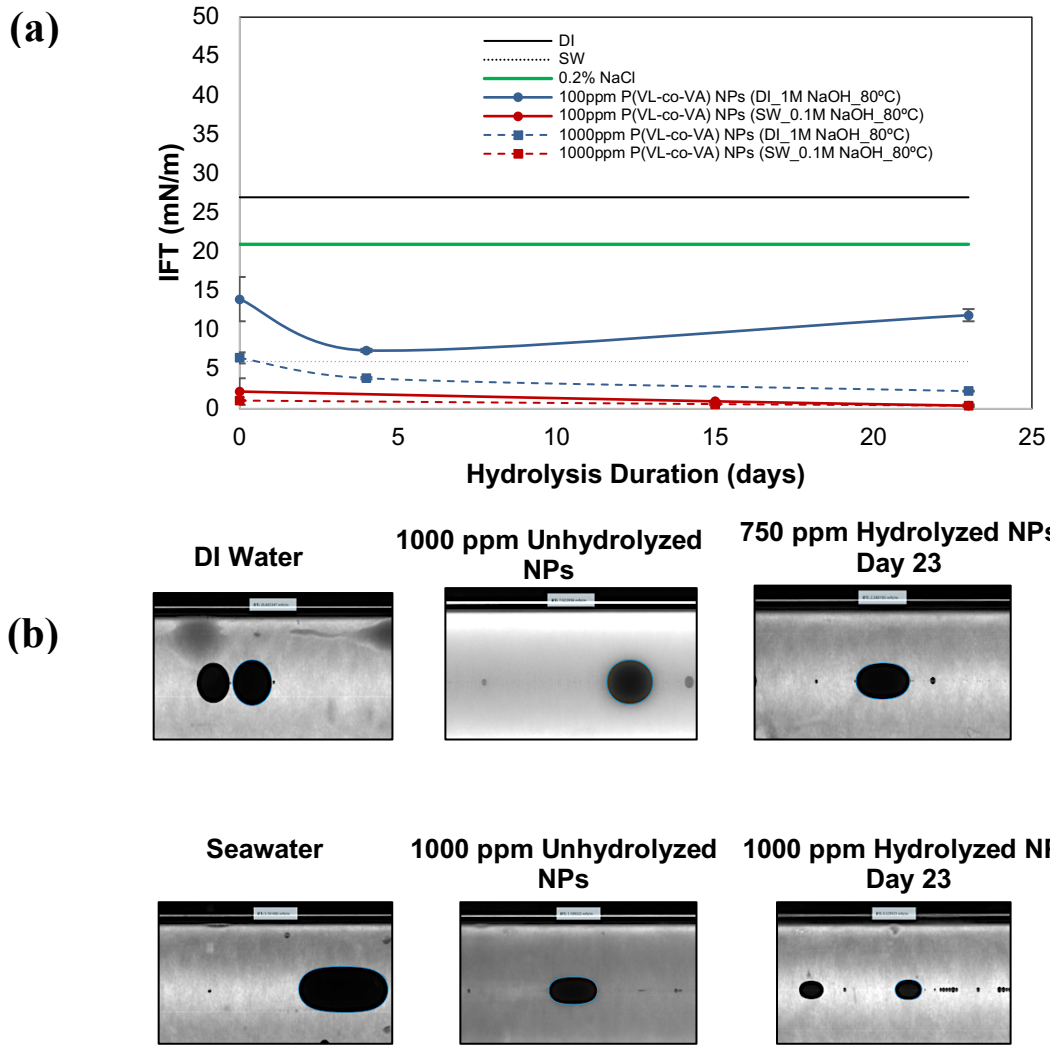
Figure 27 (a) IFT measurements of crude oil in DI water or seawater at 8000rpm in comparison to the unhydrolyzed and hydrolyzed NPs at different hydrolysis , (b) crude oil droplet image.

4.3   SUMMARY

In summary, hydrolysable p-(VL-co-VA, 3:1 molar ratio) NPs were synthesized and their efficacy for slow and controlled release of surfactant generated via hydrolysis of the ester side chain was demonstrated. The hydrolysable NPs with a size of ~ 55 nm and a zeta potential of -54 mV consist of a poly(vinyl laurate-*co*-vinyl acetate) core stabilized by a PEG shell.   Hydrolysis kinetics in an accelerated, base-catalyzed reaction show release of about 11 and 30% of available surfactant at 25 and 80°C, respectively. The corresponding values in seawater are 22 and 76%, respectively. In addition, the effectiveness of the NPs in altering the wettability of a hydrophobic, oil-wet substrate was evaluated and compared to that of neat, commercially available sodium laureate. Finally, confocal microscopy demonstrated the ability of the NPs to produce surfactant molecules in-situ and to stabilize oil-water emulsions supporting their potential applications in diverse fields including hydrocarbon recovery and oil spill remediation.

5. CHAPTER 5 : P(VL-*co*-VA) NANOPARTICLES WITH A POLY GLYCIDYL METHACRLATE (PGMA) BURSH

5.1 EXPERIMENTAL PROCEDURE

5.1.1 Synthesis of Hydrolysable Nanoparticle Seed

The hydrolysable P(VL-*co*-VA) NP core was fabricated through a free-radical emulsion copolymerization of vinyl-laurate and vinyl acetate in 3:1 molar ratio. Cetyltrimethylammonium bromide, sodium dodecyl sulfate or glycolic acid ethoxylate oleyl ether (GAEOE) and Triton X-100 were incorporated in the synthesis as either the cationic, anionic and nonionic surfactants, respectively, to obtain the most stable P(VL-co-VA) NP core that can be used in the grafting process. 0.08 g of N-dodecyl-N,N-dimethyl-3-ammonio-1-propanesulfonate zwitterionic surfactant, 0.4 g of allyloxy-2-hydroxy-1-propanesulfonic acid sodium salt solution comonomer, 0.6 mL of 2-propanol, 0.04g of sodium bicarbonate ($NaHCO_3$) and the designed percentage amount of respective surfactant (specified in Table 3) were added to 11-ml deionized-water and mixed thoroughly. 0.8mg of Nile red dye, 1.228 g of vinyl-laurate and 0.153 g of vinyl-acetate were added to the above solution under vigorous stirring to form an emulsion. 0.02 g of sodium persulfate was then added, and the emulsion was heated to 60ºC and polymerized overnight. The obtained nanoparticles were purified via dialysis (10K MWCO) for seven days with frequent water replacement yielding ~ 8wt% nanoparticle concentration.

5.1.2 Swelling Seeded Polymerization of P(VL-*co*-VA) NP core with Poly(Glycidyl Methacrylate) (PGMA) Brush (P(VL-*co*-VA)-PGMA)

The hydrolysable P(VL-*co*-VA) NP seed (25g) was dispersed in 25g DI. A monomer solution containing GMA, and DVB as a crosslinker were mixed thoroughly and 0.5ml of this solution were added to the seed mixture. 2,2′-azobis(2-methylpropionamidine) dihydrochloride (V50) used as the initiator (weight ratio V50/GMA=0.0189) was dissolved in 3ml DI and added to the seed dispersion. The mixture was kept at 60°C with mechanical stirring at 220 rpm overnight to initiate swelling. The remaining monomer solution was then added in a slow, continuous, dropwise fashion at 0.5ml/hr using a syringe pump with continuous stirring at 220 rpm at 60°C to initiate the brush polymerization.

5.1.3 P(VL-*co*-VA)-PGMA Functionalization

After the formation of P(VL-*co*-VA)-PGMA NPs, functionalization was attempted through sulfonation and amination of the epoxide ring. For sulfonation, sodium sulfite (SS) and sodium bisulfite (SBS) in 1:1 weight ratio were added in excess to the nanoparticles (four times the amount of GMA) and the mixture was stirred at 220 rpm at 80°C. For amination, 1.68 g of ethylenediamine in 4 g of DI water were added to 11 g of P(VL-*co*-VA)-PGMA NPs and stirred at 50°C for 24 hours. Next, 5ml of glycidyltrimethylammonium chloride in 5ml DI water was added to the mixture and stirred at 50°C for another 24 hours. All functionalized nanoparticles were dialyzed for two days with frequent water replacement.

5.1.4 Characterization of the P(VL-*co*-VA)-PGMA Brush Nanoparticles

The nanoparticle size and zeta potential in deionized water at 25°C were determined via dynamic light scattering (DLS) using a Zeta Nanosizer (Malven Instruments,

UK). Scanning Electron Microscopy (SEM) and Transmission Electron Microscopy (TEM) were obrtaineed on a Tescan Mira3 FESEM and Zeiss Gemini 500 SEM and FEI Tecnai 12 BioTwin TEM, respectively.

5.1.5 Assessment Of P(VL-*Co*-VA)-PGMA Nps Stability in High Salinity Water (HSW) at High Temperature

To evaluate the nanoparticle stability in high salinity water, 1% from the nanoparticle suspension was dispersed in HSW (composition in Table 2) and kept at 80ºC with daily size measurements.

Table 2 Salt composition to formulate High Salinity Water (HSW) used in the NPs stability test

Salt	NaCl	$CaCl_2.2H_2O$	$MgCl_2.6H_2O$	Na_2SO_4	$BaCl_2$	$NaHCO_3$
Concentration (g/L)	74.59	49.79	13.17	0.6	0.01	0.51

5.1.6 Assessment Of Targeted Delivery Using Laser Confocal Scanning Microscopy (LCSM)

For confocal microscopy imaging, the patterned nanoparticle suspension was mixed with model oil (0.01M stearic acid in hexadecane) in equivolumetric amounts. Few millimeters of the mixture were placed on a glass slide on the microscope objective for imaging.

5.2 RESULTS AND DISCUSSION

5.2.1 Nanoparticle Characterization.

5.2.1.1 *P(VL-co-VA) Nanoparticle Core*

N-2 (10wt% P(VL-co-VA) NPs + 2%GAEOE) (Table 3) was selected as the core particle in all following experiments as the alternative surfactants either exhibited instant aggregation or phase separation overtime. The P(VL-co-VA) NP

core was scaled-up to prepare a 400ml batch and characterized by DLS, TEM and SEM (Figure 28) all of which confirm the formation of spherical P(VL-co-VA) NPs that are 30 ± 2.7 nm in size (PDI =0.135) with zeta potential of -15 mV.

Table 3 Nanoparticle composition, size and zeta potential synthesized with different cationic, anionic, and nonionic surfactants and varying monomer concentrations.

NP Composition *	Size (nm)	Zeta Potential (mV)
N-1: 5wt% P(VL-co-VA) + 2% GAEOE	18	-10
N-2: 10wt% P(VL-co-VA) + 2% GAEOE	30	-15
N-3: 5wt% P(VL-co-VA) + 2% CTAB	Aggregation	
N-4: 5wt% P(VL-co-VA) + 3% CTAB	Aggregation	
N-5: 10wt% P(VL-co-VA) + 6% CTAB	35	11
N-6: 5wt% P(VL-co-VA) + 1.5% SDS + 1.5% TX-100	20	-22
N-7: 5wt% P(VL-co-VA) + 1.5% CTAB + 1.5% TX-100	15	14
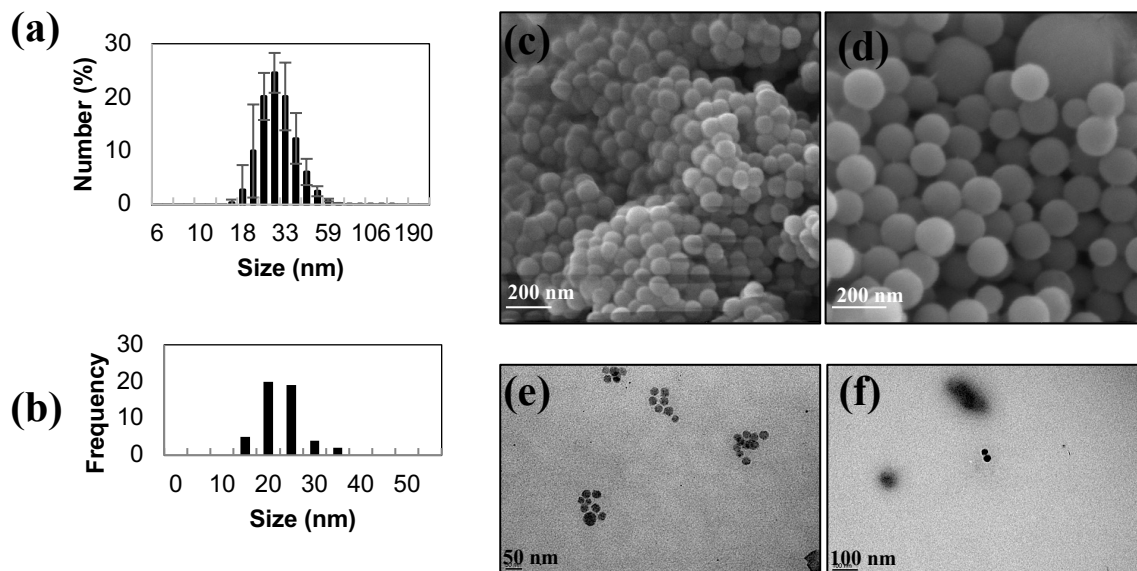
Figure 28 (a) Size distribution from DLS measurement of P(VL-co-VA) NP core, (b) size distribution from TEM analysis of P(VL-co-VA) NP core. (c) and (d) SEM images of P(VL-co-VA) NP core . Scale bar: 200 nm for (c) and (d). (e) and (f) TEM images of P(VL-co-VA) NP core. Scale bar: 50nm for (d) and 100nm for (e).

At the initial screening stage, the amount of GMA monomer and DVB crosslinker were varied (Table 4) and nanoparticle size distribution was recorded to establish a baseline criterion for selecting the optimized system with enhanced NPs stability. As observed from Table 4, when increasing the ratio of GMA to NP (S-4, S-6, S-7) nanoparticle aggregation is observed. On the contrary, for the lowest GMA/NP ratio (S-5), minimal alteration to the core was observed. Hence, S-1, S-3 and S-9 were selected for electron microscope imaging to examine the NPs surface morphology.

Table 4 Size measurements of P(VL-co-VA) NPs grafted with PGMA at varying monomer and crosslinker ratios.

Sample	GMA/NP wt. ratio	DVB/NP (%)	Size (nm)	PDI
S-1	0.825	0.56	50	0.132
S-2	1.03	1	68	0.063
S-3	1.2	1.8	80	0.059
S-4	1.32	0.25	-	-
S-5	0.625	1.8	40	0.34
S-6	2.40	1.8		-
S-7*	1.2	1.8		-
S-8*	1.2	2.5	132	0.073
S-9	1.625	2.5	125	0.034

0.02g of initiator added during the dropwise feeding of the monomer solution

Electron microscopy images (Figure 30) show that the growth of PGMA on the P(VL-co-VA) core is asymmetric due to the phase separation and leads to the formation of either "peanut" or aggregates of multiple cores morphologies. Compared to other "living" radical polymerization methods, free-radical seeded polymerization provided little control of the PGMA growth behavior on the P(VL-co-VA) NP core.[126,127] It is worth noting that increasing the crosslink density (S-3 to S-9), leads to the formation of head-tail structures, where PGMA continues to grow away from the NP core. Hence, the subsequent functionalization of the NPs (via amination or sulfonation) leads to non-uniform distribution of charge and localizing the charge on the PGMA side, which may adversely impact the

nanoparticle stability (Figure 29). The asymmetric PGMA coverage, which acts as a surfactant when functionalized, leads to nanoparticle agglomeration. Such behavior was observed by Xu et al.[128], when low amount of Gemini surfactant is used in the stabilization of AuNPs. S-3, with zeta potential of -58mV, was selected for further functionalization due to the smaller size, highly-negative zeta potential and less asymmetric growth.[128]
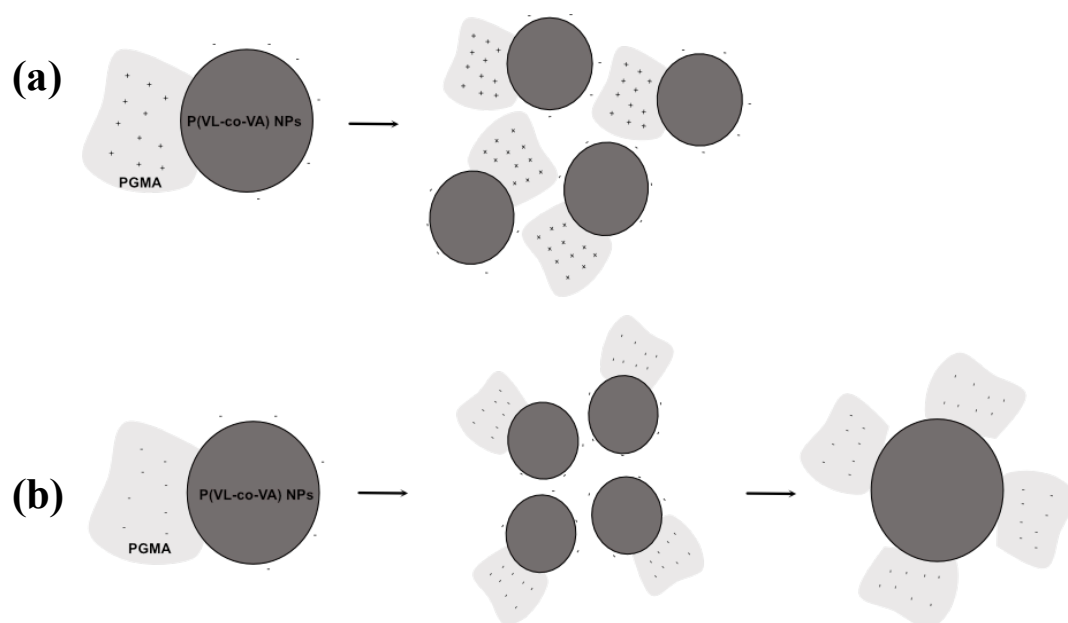
Figure 29 Schematic of various nanoparticle assemblies of (a) aminated P(VL-co-VA)-PGMA NPs, (b) sulfonated P(VL-co-VA)-PGMA NPs (Adopted from Xu et al. 125).

(S-1)

(S-3)

(S-9)
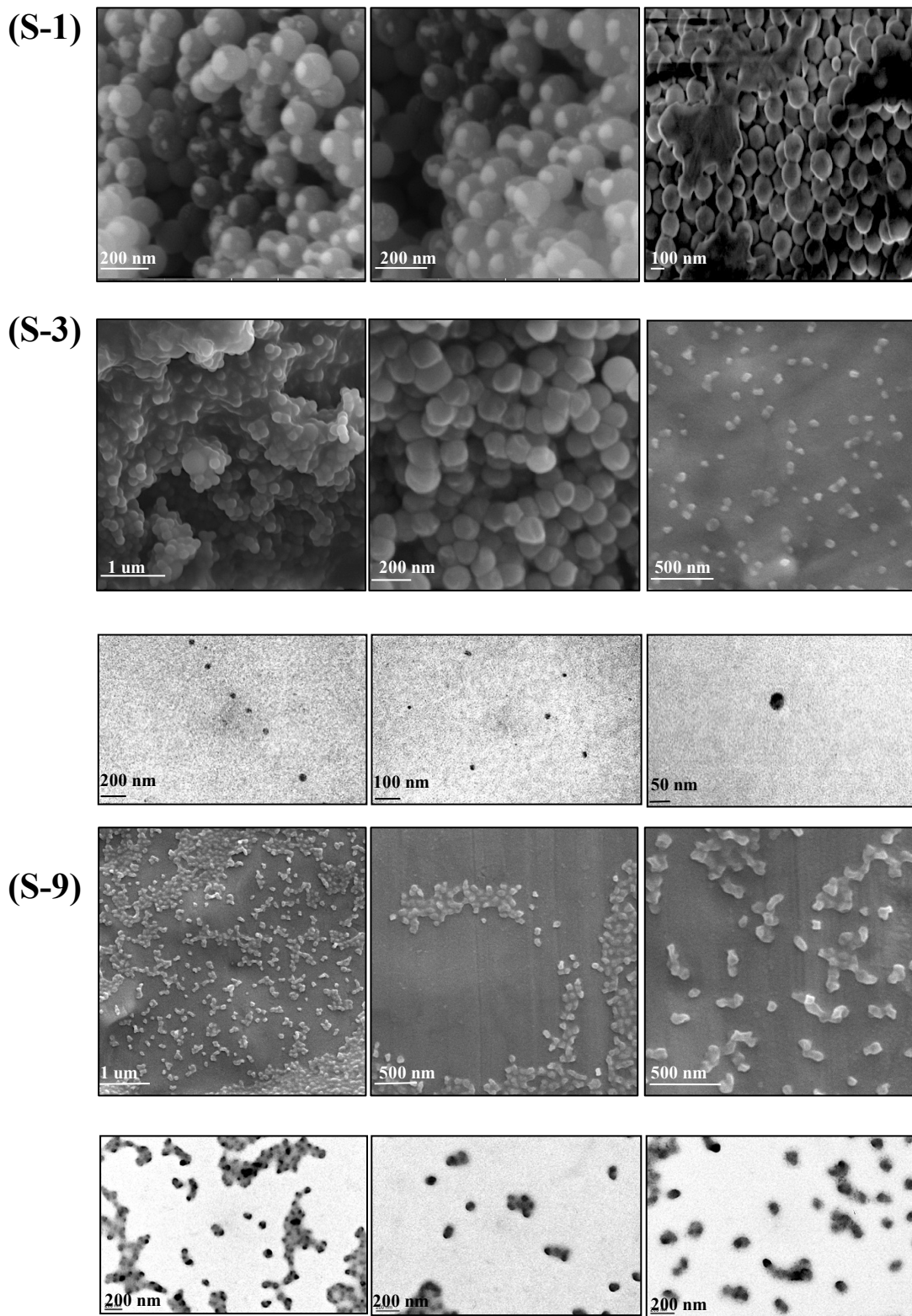
Figure 30 SEM and TEM images of S-1, S-3 and S-9 P(VL-co-VA) NPs grafted with PGMA

5.2.2 Assessment of P(VL-co-VA)-PGMA NPs Stability in High Salinity Water

Untreated, *unfunctionalized* S-3 was tested for stability in HSW and the results are summarized in Table 5. Despite the high negative charge without sulfonation, the nanoparticles experience aggregation when placed in HSW (from 80nm in DI water to 253nm in HSW at 80ºC) after one day as seen in Figure 31. Further aggregation is observed visually after day one.

Table 5 Size measurements of unfunctionalized P(VL-co-VA)-PGMA NPs in DI and HSW

Recipe	Size (nm) DI	Zeta Potential (mV) DI	Size (nm), HSW 80ºC Day (1)
P(VL-co-VA)-PGMA NPs (S-3)	80	-58	253
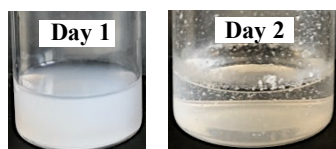
Figure 31 Unfunctionalized P(VL-co-VA)-PGMA NPs in HSW at 80ºC

The subsequent functionalization through sulfonation did not yield a stable colloidal system, which is attributed to the charge localization on one side as discussed earlier. Aminating the NPs reduced the zeta potential from -58 to a neutral value (Table 6), which induces the aggregation even in DI water (Figure 32).

Table 6 Size measurements and zeta potential values for functionalized P(VL-co-VA)-PGMA NPs

Recipe	Size (nm) DI	Zeta Potential (mV) DI	Size (nm), HSW 80ºC Day (1)
(-) S-3	166	-35	839
(+) S-3	95	~0	-
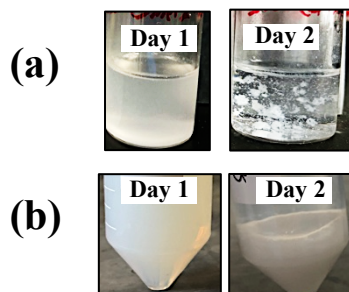
Figure 32 (a) Sulfonated P(VL-co-VA)-PGMA NPs in HSW at 80ºC, (b) Aminated P(VL-co-VA)-PGMA NPs as synthesized in DI water

5.2.3 Assessment of P(VL-co-VA)-PGMA NPs for Targeted Delivery of Surfactants

As observed from the morphology of P(VL-co-VA)-PGMA NPs, the doublet structure suggests the formation of "Janus" particles with a hydrophobic nanoparticle core and a more hydrophilic PGMA side. Confocal microscopy imaging was conducted to assess the potential of using P(VL-co-VA)-PGMA NPs for targeted delivery applications in oil-water mixtures. The proposed targeted delivery method for the untreated P(VL-co-VA)-PGMA NPs is through the hydrophobic nanoparticle core assembly in the oil phase and the hydrophilic PGMA assembly in the aqueous phase. The proposed targeted delivery mechanism for the aminated P(VL-co-VA)-PGMA NPs capitalizes on the electrostatic interaction between the aminated PGMA side and the negatively charged, carboxylate-terminated oil phase (Figure 33).
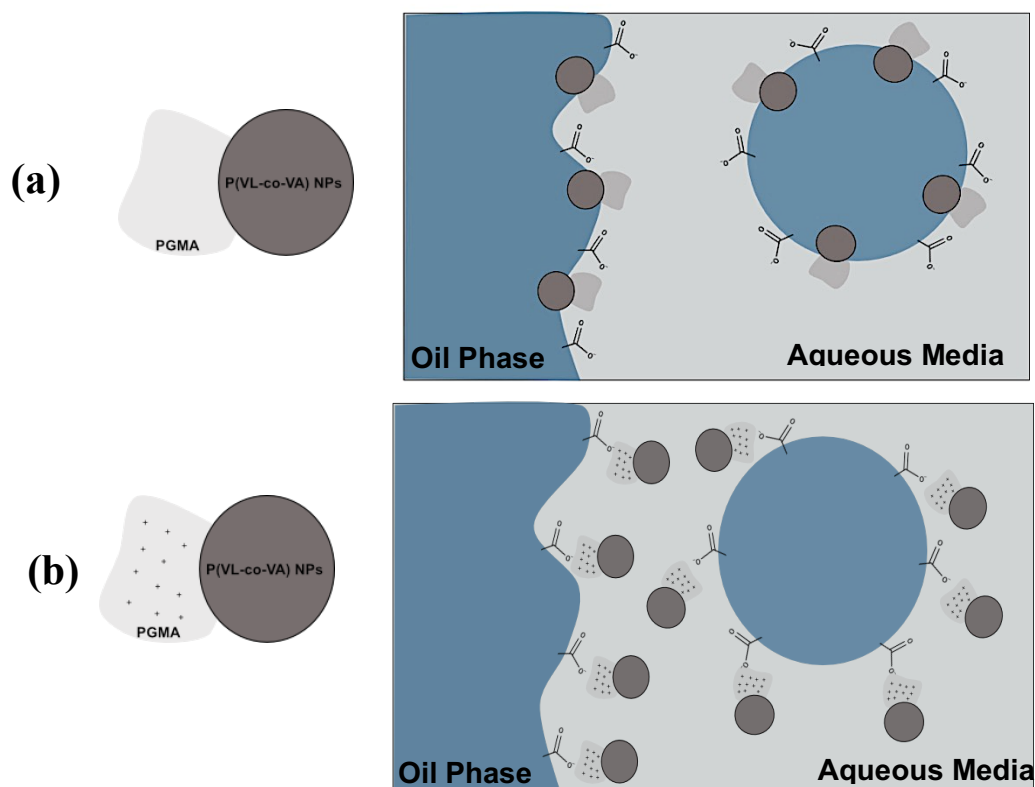
Figure 33 Schematic of the delivery mechanism of P(VL-co-VA) NPs grafted with PGMA, (a) untreated P(VL-co-VA)-PGMA NPs amphiphilic assembly, (b) aminated P(VL-co-VA)-PGMA NPs assembly via electrostatic interactions.

5.2.3.1 *Untreated P(VL-co-VA)-PGMA NPs*

Preliminary confocal microscopy images for P(VL-co-VA) NP core dispersion in the presence of model oil prior to PGMA grafting are shown in Figure 34.a. There is no preferential adsorption of the NPs at the oil-water interface, where they appear dispersed mainly in the aqueous phase. On the contrary, for the P(VL-co-VA)-PGMA NPs (Figure 34.b), there is an increased tendency of the NPs to be dispersed in the oil phase.

(a)
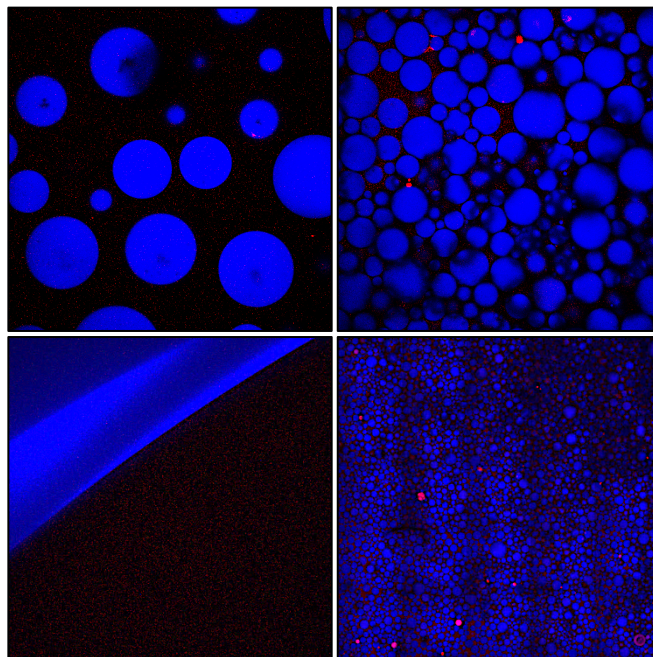
(b)
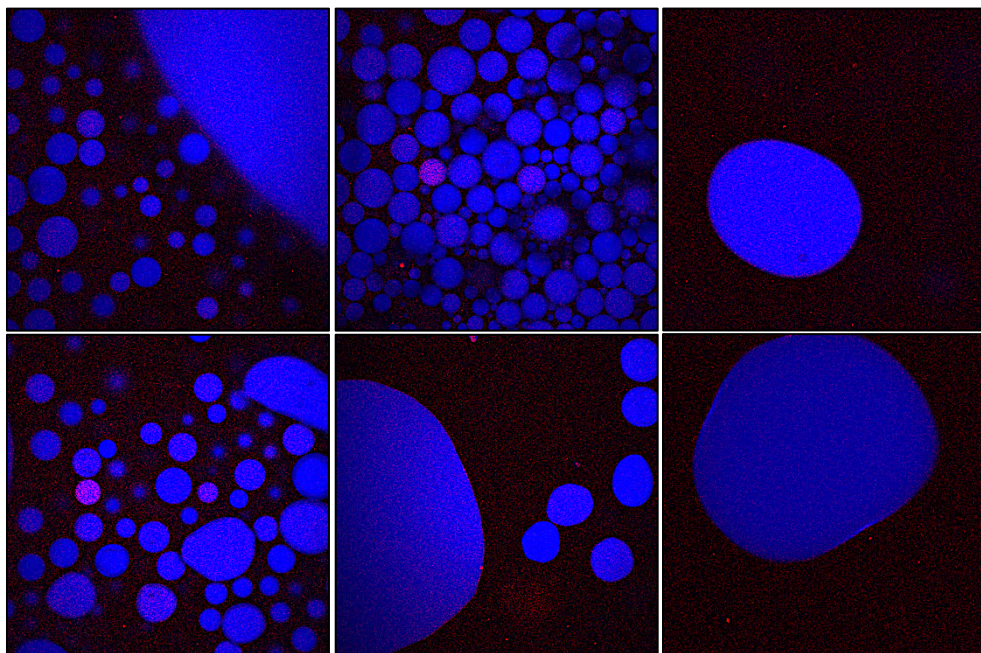
Figure 34 Confocal microscopy images of emulsions prepared by vortexing equivolumetric amounts of model oil and (a) P(VL-co-VA) NP core suspension, (b) P(VL-co-VA)-PGMA NP suspension

Confocal micrographs for the aminated P(VL-co-VA)-PGMA NPs (Figure 35) demonstrate the nanoparticles assembly at the oil-water interface. This assembly is facilitated by the electrostatic interactions of the carboxylic group present in model oil and the ammonium groups present in PGMA.
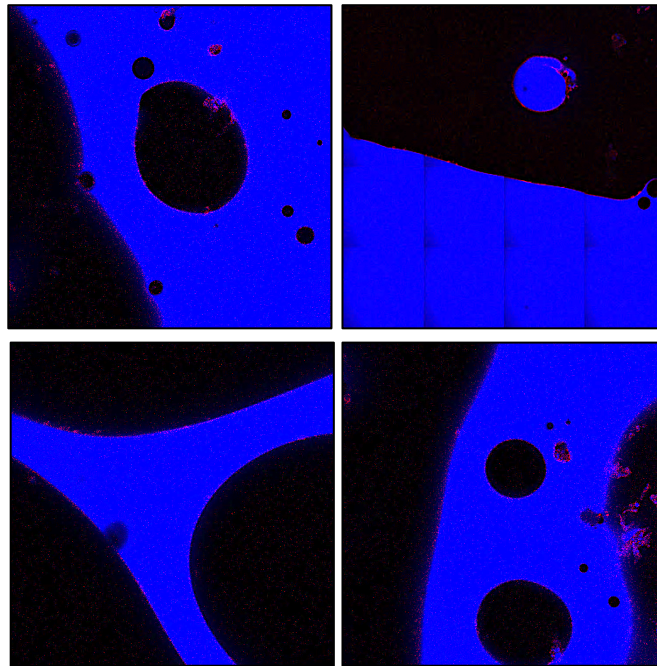
Figure 35 Confocal micrographs of emulsions prepared by vortexing equivolumetric amounts of model oil and aminated P(VL-co-VA)-PGMA NPs

5.3 SUMMARY

In summary, P(VL-co-VA) NP core was synthesized using glycolic acid ethoxylate oleyl ether (GAEOE) as the surfactant yielding NPs that are ~30 nm in size with a zeta potential of -15mV. PGMA was grafted using seeded free-radical emulsion polymerization with 1.2 GMA/NP wt. ratio and 1.2% DVB/NP as a crosslinker. The grafted P(VL-co-VA)-PGMA NPs show an increase in size to 80 nm and zeta potential of -58. Electron microscopy images demonstrate either an asymmetric growth of PGMA

on the P(VL-co-VA) NPs on one side or P(VL-co-VA) NPs aggregates glued together by PGMA. Subsequent functionalization through sulfonation or amination result in increased size to 166 nm and 95 nm with zeta potential of -35 and ~0 mV, respectively. The system requires further optimization to enhance the stability in high-salinity water (HSW). The P(VL-co-VA)-PGMA NPs were tested for targeted delivery in oil-water emulsions. The untreated P(VL-co-VA)-PGMA NPs show increased tendency to disperse in the oil phase whereas the aminated P(VL-co-VA)-PGMA NPs assemble at the oil-water interface due to the weak electrostatic interactions between the carboxylic groups in model oil and ammonium groups in PGMA as well as H-bonding.

6. CHAPTER 6: CONCLUSIONS AND FUTURE DIRECTION

In conclusion, this study demonstrated the synthesis of a stimuli-responsive, hydrolysable poly(vinyl laurate-co-vinyl acetate), P(VL-co-VA), nanoparticle platform for the slow and controlled-release of surfactants. The system comprises a nanoparticle core synthesized by the free-radical emulsion copolymerization of vinyl laurate and vinyl acetate core grafted with either a poly(ethylene-glycol), PEG, or poly(glycidyl methacrylate), PGMA, on the surface. The slow and controlled release behavior of the PEGylated system in an accelerated, base-catalyzed reaction was demonstrated. The study further demonstrated the surfactancy of the platform and its ability to be utilized in various interfacial applications including wettability alteration, stabilization of emulsions, generation of foam and lowering the interfacial tension (IFT). This thesis also explored the potential of enhancing the system's stability in high salinity conditions by the PGMA graft yielding polymeric brushes with multiple charges and allowing for both electrostatic and steric stabilization. Future work can be invested in controlling the anchoring behavior of PGMA on P(VL-co-VA) NPs for a uniform brush distribution. Surface-initiated, controlled radical polymerization methods (SI-CRP)[129] can be considered to hinder the asymmetric PGMA growth observed in the seeded polymerization. The subsequent functionalization of the epoxy groups in PGMA can allow the system to be utilized in the targeted delivery of the nanoparticles to the oil phase in oil-water mixtures. The targeted delivery of surfactants is advantageous considering the expensive implementation of neat, systemic surfactant flooding operations that are normally expended at regions close to the injection site with limited availability in deep reservoir zones.

7. REFERENCES

(1)   Mao, X.; Jiang, R.; Xiao, W.; Yu, J. Use of Surfactants for the Remediation of Contaminated Soils: A Review. *Journal of Hazardous Materials*. Elsevier B.V. March 1, 2015, pp 419–435. https://doi.org/10.1016/j.jhazmat.2014.12.009.

(2)   Baglioni, M.; Guaragnone, T.; Mastrangelo, R.; Sekine, F. H.; Ogura, T.; Ogura, T.; Ogura, T.; Baglioni, P. Nonionic Surfactants for the Cleaning of Works of Art: Insights on Acrylic Polymer Films Dewetting and Artificial Soil Removal. *ACS Appl. Mater. Interfaces* **2020**, *12* (23), 26704–26716. https://doi.org/10.1021/acsami.0c06425.

(3)   Pal, S.; Mushtaq, M.; Banat, F.; Al Sumaiti, A. M. Review of Surfactant-Assisted Chemical Enhanced Oil Recovery for Carbonate Reservoirs: Challenges and Future Perspectives. *Pet. Sci.* **2018**, *15* (1), 77–102. https://doi.org/10.1007/s12182-017-0198-6.

(4)   Nourafkan, E.; Hu, Z.; Wen, D. Nanoparticle-Enabled Delivery of Surfactants in Porous Media. *J. Colloid Interface Sci.* **2018**, *519*, 44–57. https://doi.org/10.1016/j.jcis.2018.02.032.

(5)   De Avila, J. N. L.; De Araujo, L. L. G. C.; Drexler, S.; De Almeida Rodrigues, J.; Nascimento, R. S. V. Polystyrene Nanoparticles as Surfactant Carriers for Enhanced Oil Recovery. *J. Appl. Polym. Sci.* **2016**, *133* (32). https://doi.org/10.1002/app.43789.

(6)   de Freitas, F. A.; Keils, D.; Lachter, E. R.; Maia, C. E. B.; Pais da Silva, M. I.;

Veiga Nascimento, R. S. Synthesis and Evaluation of the Potential of Nonionic Surfactants/Mesoporous Silica Systems as Nanocarriers for Surfactant Controlled Release in Enhanced Oil Recovery. *Fuel* **2019**, *241* (February 2018), 1184–1194. https://doi.org/10.1016/j.fuel.2018.12.059.

(7)   El Achouri, M.; Kertit, S.; Gouttaya, H. M.; Nciri, B.; Bensouda, Y.; Perez, L.; Infante, M. R.; Elkacemi, K. Corrosion Inhibition of Iron in 1 M HCl by Some Gemini Surfactants in the Series of Alkanediyl-α,ω-Bis-(Dimethyl Tetradecyl Ammonium Bromide). *Prog. Org. Coatings* **2001**, *43* (4), 267–273. https://doi.org/10.1016/S0300-9440(01)00208-9.

(8)   Nafisi, S.; Maibach, H. I. Nanotechnology in Cosmetics. In *Cosmetic Science and Technology: Theoretical Principles and Applications*; 2017; pp 337–361. https://doi.org/10.1016/B978-0-12-802005-0.00022-7.

(9)   Deng, Y.; Zheng, X.; Bai, Y.; Wang, Q.; Zhao, J.; Huang, J. Surfactant-Controlled Ink Drying Enables High-Speed Deposition of Perovskite Films for Efficient Photovoltaic Modules. *Nat. Energy* **2018**, *3* (7), 560–566. https://doi.org/10.1038/s41560-018-0153-9.

(10)   Weiszhár, Z.; Czúcz, J.; Révész, C.; Rosivall, L.; Szebeni, J.; Rozsnyay, Z. Complement Activation by Polyethoxylated Pharmaceutical Surfactants: Cremophor-EL, Tween-80 and Tween-20. *Eur. J. Pharm. Sci.* **2012**, *45* (4), 492–498. https://doi.org/10.1016/j.ejps.2011.09.016.

(11)   Lawrence, M. J. Surfactant Systems: Their Use in Drug Delivery. *Chemical*

Society Reviews. 1994, pp 417–424. https://doi.org/10.1039/CS9942300417.

(12)   Müllertz, A.; Ogbonna, A.; Ren, S.; Rades, T. New Perspectives on Lipid and

Surfactant Based Drug Delivery Systems for Oral Delivery of Poorly Soluble

Drugs. *Journal of Pharmacy and Pharmacology*. 2010, pp 1622–1636.

https://doi.org/10.1111/j.2042-7158.2010.01107.x.

(13)   Sheng, J. J. Surfactant Enhanced Oil Recovery in Carbonate Reservoirs.

Enhanc. Oil Recover. F. Case Stud. **2013**, *6* (June), 281–299.

https://doi.org/10.1016/B978-0-12-386545-8.00012-9.

(14)   Tangirala, S.; Sheng, J. J. Roles of Surfactants during Soaking and Post Leak-

Off Production Stages of Hydraulic Fracturing Operation in Tight Oil-Wet

Rocks. *Energy and Fuels* **2019**, *33* (9), 8363–8373.

https://doi.org/10.1021/acs.energyfuels.9b01913.

(15)   Raney, K. H.; Miller, C. A. Optimum Detergency Conditions with Nonionic

Surfactants. *J. Colloid Interface Sci.* **1987**, *119* (2), 539–549.

https://doi.org/10.1016/0021-9797(87)90301-8.

(16)   Scheibel, J. J. The Evolution of Anionic Surfactant Technology to Meet the

Requirements of the Laundry Detergent Industry. *Journal of Surfactants and

Detergents*. 2004, pp 319–328. https://doi.org/10.1007/s11743-004-0317-7.

(17)   Zembyla, M.; Murray, B. S.; Sarkar, A. Water-in-Oil Emulsions Stabilized by

Surfactants, Biopolymers and/or Particles: A Review. *Trends Food Sci.

Technol.* **2020**, *104* (January), 49–59. https://doi.org/10.1016/j.tifs.2020.07.028.

(18)   Bonnaud, M.; Weiss, J.; McClements, D. J. Interaction of a Food-Grade Cationic Surfactant (Lauric Arginate) with Food-Grade Biopolymers (Pectin, Carrageenan, Xanthan, Alginate, Dextran, and Chitosan). *J. Agric. Food Chem.* **2010**, *58* (17), 9770–9777. https://doi.org/10.1021/jf101309h.

(19)   Venzmer, J. Superspreading - 20years of Physicochemical Research. *Curr. Opin. Colloid Interface Sci.* **2011**, *16* (4), 335–343. https://doi.org/10.1016/j.cocis.2010.11.006.

(20)   Morrow, N. R.; Mason, G. Recovery of Oil by Spontaneous Imbibition. *Curr. Opin. Colloid Interface Sci.* **2001**, *6* (4), 321–337. https://doi.org/10.1016/S1359-0294(01)00100-5.

(21)   Kamari, A.; Sattari, M.; Mohammadi, A. H.; Ramjugernath, D. Reliable Method for the Determination of Surfactant Retention in Porous Media during Chemical Flooding Oil Recovery. *Fuel* **2015**, *158*, 122–128. https://doi.org/10.1016/j.fuel.2015.05.013.

(22)   Shahzad Kamal, M.; Hussein, I. A.; Sultan, A. S. Review on Surfactant Flooding: Phase Behavior, Retention, IFT, and Field Applications. **2017**. https://doi.org/10.1021/acs.energyfuels.7b00353.

(23)   Weston, J. S.; Harwell, J. H.; Shiau, B. J.; Kabir, M. Disrupting Admicelle Formation and Preventing Surfactant Adsorption on Metal Oxide Surfaces Using Sacrificial Polyelectrolytes. *Langmuir* **2014**, *30* (22), 6384–6388. https://doi.org/10.1021/la501074x.

(24)   Falcone, J. S.; Krumrine, P. H.; Schweiker, G. C. The Use of Inorganic

Sacrificial Agents in Combination with Surfactants in Enhanced Oil Recovery.

J. Am. Oil Chem. Soc. **1982**, *59* (10). https://doi.org/10.1007/BF02634449.

(25)   Huo, Q.; Margolese, D. I.; Stucky, G. D. Surfactant Control of Phases in the

Synthesis of Mesoporous Silica-Based Materials. *Chem. Mater.* **1996**, *8* (5),

1147–1160. https://doi.org/10.1021/cm960137h.

(26)   Shah, A.; Shahzad, S.; Munir, A.; Nadagouda, M. N.; Khan, G. S.; Shams, D.

F.; Dionysiou, D. D.; Rana, U. A. Micelles as Soil and Water Decontamination

Agents. *Chemical Reviews*. American Chemical Society May 25, 2016, pp

6042–6074. https://doi.org/10.1021/acs.chemrev.6b00132.

(27)   Shaban, S. M.; Kang, J.; Kim, D. H. Surfactants: Recent Advances and Their

Applications. *Compos. Commun.* **2020**, *22* (October), 100537.

https://doi.org/10.1016/j.coco.2020.100537.

(28)   Harikrishnan, A. R.; Dhar, P.; Agnihotri, P. K.; Gedupudi, S.; Das, S. K.

Wettability of Complex Fluids and Surfactant Capped Nanoparticle-Induced

Quasi-Universal Wetting Behavior. *J. Phys. Chem. B* **2017**, *121* (24), 6081–

6095. https://doi.org/10.1021/acs.jpcb.7b02723.

(29)   Seymour, K. G. Surfactants and Interfacial Phenomena. *J. AOAC Int.* **1979**.

https://doi.org/10.1093/jaoac/62.3.700.

(30)   Bormashenko, E. Y. *Physics of Wetting*; 2017.

https://doi.org/10.1515/9783110444810.

(31) Sonia, T. A.; Sharma, C. P. Experimental Techniques Involved in the Development of Oral Insulin Carriers. In *Oral Delivery of Insulin*; 2014; pp 169–217. https://doi.org/10.1533/9781908818683.169.

(32) Mohammadi, R.; Wassink, J.; Amirfazli, A. Effect of Surfactants on Wetting of Super-Hydrophobic Surfaces. *Langmuir* **2004**. https://doi.org/10.1021/la049268k.

(33) Hauner, I. M.; Deblais, A.; Beattie, J. K.; Kellay, H.; Bonn, D. The Dynamic Surface Tension of Water. *J. Phys. Chem. Lett.* **2017**. https://doi.org/10.1021/acs.jpclett.7b00267.

(34) Jarrahian, K.; Seiedi, O.; Sheykhan, M.; Sefti, M. V.; Ayatollahi, S. Wettability Alteration of Carbonate Rocks by Surfactants: A Mechanistic Study. *Colloids Surfaces A Physicochem. Eng. Asp.* **2012**, *410*, 1–10. https://doi.org/10.1016/j.colsurfa.2012.06.007.

(35) Standnes, D. C.; Austad, T. Wettability Alteration in Chalk. *J. Pet. Sci. Eng.* **2000**, *28* (3), 123–143. https://doi.org/10.1016/s0920-4105(00)00084-x.

(36) Preuss, M.; Butt, H. J. Direct Measurement of Particle-Bubble Interactions in Aqueous Electrolyte: Dependence on Surfactant. *Langmuir* **1998**. https://doi.org/10.1021/la971349b.

(37) Xu, Q.; Nakajima, M.; Ichikawa, S.; Nakamura, N.; Roy, P.; Okadome, H.; Shiina, T. Effects of Surfactant and Electrolyte Concentrations on Bubble Formation and Stabilization. *J. Colloid Interface Sci.* **2009**.

https://doi.org/10.1016/j.jcis.2008.12.044.

(38)   Mitra, S.; Dungan, S. R. Micellar Properties of Quillaja Saponin. 1. Effects of

Temperature, Salt, and PH on Solution Properties. *J. Agric. Food Chem.* **1997**.

https://doi.org/10.1021/jf960349z.

(39)   Coupland, J. N.; Sigfusson, H. Food Emulsions. In *Handbook of Food Science,*

Technology, and Engineering - 4 Volume Set; 2005.

https://doi.org/10.1201/9781420029581.ch9.

(40)   Sjoblom, J. Emulsions and Emulsion Stability: Surfactant Science Series/61.

CRC Press **2005**.

(41)   Pouton, C. W. Formulation of Self-Emulsifying Drug Delivery Systems.

Advanced Drug Delivery Reviews. 1997. https://doi.org/10.1016/S0169-

409X(96)00490-5.

(42)   Fingas, M.; Fieldhouse, B. Water-in-Oil Emulsions: Formation and Prediction.

In *Proceedings of the 34th AMOP Technical Seminar on Environmental*

Contamination and Response; 2011.

https://doi.org/10.14355/jpsr.2014.0301.04.

(43)   Alvarado, V.; Wang, X.; Moradi, M. Stability Proxies for Water-in-Oil

Emulsions and Implications in Aqueous-Based Enhanced Oil Recovery.

Energies. 2011. https://doi.org/10.3390/en407105.

(44)   Goodarzi, F.; Zendehboudi, S. A Comprehensive Review on Emulsions and

Emulsion Stability in Chemical and Energy Industries. *Can. J. Chem. Eng.* **2019**. https://doi.org/10.1002/cjce.23336.

(45)   Blomberg, E.; Poptoshev, E.; Claesson, P. Surface Forces and Emulsion Stability. In *Encyclopedic Handbook of Emulsion Technology*; 2001. https://doi.org/10.1201/9781420029581.ch13.

(46)   Katepalli, H.; Bose, A. Response of Surfactant Stabilized Oil-in-Water Emulsions to the Addition of Particles in an Aqueous Suspension. *Langmuir* **2014**. https://doi.org/10.1021/la502291q.

(47)   Binks, B. P.; Rodrigues, J. A.; Frith, W. J. Synergistic Interaction in Emulsions Stabilized by a Mixture of Silica Nanoparticles and Cationic Surfactant. *Langmuir* **2007**. https://doi.org/10.1021/la0634600.

(48)   Mulqueen, P. Recent Advances in Agrochemical Formulation. *Adv. Colloid Interface Sci.* **2003**. https://doi.org/10.1016/S0001-8686(03)00106-4.

(49)   Acosta, E. J.; Yuan, J. S.; Bhakta, A. S. The Characteristic Curvature of Ionic Surfactants. *J. Surfactants Deterg.* **2008**. https://doi.org/10.1007/s11743-008-1065-7.

(50)   Ekserova, D. R.; Krugliakov, P. M. *Foam and Foam Films: Theory, Experiment, Application*; 1998.

(51)   Rosen, M. J.; Solash, J. Factors Affecting Initial Foam Height in the Ross-Miles Foam Test. *J. Am. Oil Chem. Soc.* **1969**. https://doi.org/10.1007/BF02545623.

(52)   Murray, B. S.; Ettelaie, R. Foam Stability: Proteins and Nanoparticles. *Current*

         Opinion in Colloid and Interface Science. 2004.

         https://doi.org/10.1016/j.cocis.2004.09.004.

(53)   Exerowa, D.; Zacharieva, M.; Cohen, R.; Platikanov, D. Dependence of the

         Equilibrium Thickness and Double Layer Potential of Foam Films on the

         Surfactant Concentration. *Colloid Polym. Sci. Kolloid-Zeitschrift Zeitschrift für*

         Polym. **1979**. https://doi.org/10.1007/BF01761121.

(54)   Scriven, L. E.; Sternling, C. V. The Marangoni Effects. *Nature* **1960**.

         https://doi.org/10.1038/187186a0.

(55)   John Wiley & Sons. Kirk-Othmer Food and Feed Technology,. In *Kirk-Othmer*

         Food and Feed Technology; 2007.

(56)   Schramm, L. L.; Green, W. H. F. The Influence of Marangoni Surface Elasticity

         on Gas Mobility Reductions by Foams in Porous Media. *Colloids Surfaces A*

         Physicochem. Eng. Asp. **1995**, *94* (1), 13–28. https://doi.org/10.1016/0927-

         7757(94)02997-7.

(57)   Shepherd, M. Factors Influencing Recovery from Oil and Gas Fields. In *Oil*

         Field Production Geology; American Association of Petroleum Geologists,

         2020; pp 37–46. https://doi.org/10.1306/13161187m913372.

(58)   Alagorni, A. H.; Yaacob, Z. Bin; Nour, A. H. An Overview of Oil Production

         Stages: Enhanced Oil Recovery Techniques and Nitrogen Injection. *Int. J.*

         Environ. Sci. Dev. **2015**, *6* (9). https://doi.org/10.7763/IJESD.2015.V6.682.

(59)   Taber, J. J. RESEARCH ON ENHANCED OIL RECOVERY: PAST,

        PRESENT AND FUTURE.; Plenum Press, 1981; pp 13–52.

        https://doi.org/10.1007/978-1-4757-0337-5_2.

(60)   Gbadamosi, A. O.; Junin, R.; Manan, M. A.; Agi, A.; Yusuff, A. S. An

        Overview of Chemical Enhanced Oil Recovery: Recent Advances and

        Prospects. *Int. Nano Lett.* **2019**. https://doi.org/10.1007/s40089-019-0272-8.

(61)   Salehi, M.; Johnson, S. J.; Liang, J. T. Mechanistic Study of Wettability

        Alteration Using Surfactants with Applications in Naturally Fractured

        Reservoirs. *Langmuir* **2008**, *24* (24), 14099–14107.

        https://doi.org/10.1021/la802464u.

(62)   Aghaeifar, Z.; Strand, S.; Puntervold, T. Significance of Capillary Forces

        during Low-Rate Waterflooding. *Energy and Fuels* **2019**.

        https://doi.org/10.1021/acs.energyfuels.9b00023.

(63)   Satter, A.; Iqbal, G. M. Waterflooding and Waterflood Surveillance. In

        Reservoir Engineering; 2016. https://doi.org/10.1016/b978-0-12-800219-

        3.00016-4.

(64)   Kamal, M. S.; Hussein, I. A.; Sultan, A. S. Review on Surfactant Flooding:

        Phase Behavior, Retention, IFT, and Field Applications. *Energy and Fuels*.

        2017. https://doi.org/10.1021/acs.energyfuels.7b00353.

(65)   Lu, J.; Goudarzi, A.; Chen, P.; Kim, D. H.; Delshad, M.; Mohanty, K. K.;

        Sepehrnoori, K.; Weerasooriya, U. P.; Pope, G. A. Enhanced Oil Recovery

from High-Temperature, High-Salinity Naturally Fractured Carbonate Reservoirs by Surfactant Flood. *J. Pet. Sci. Eng.* **2014**. https://doi.org/10.1016/j.petrol.2014.10.016.

(66)   Bataweel, M. A.; Nasr-El-Din, H. A. Alternatives to Minimize Scale Precipitation in Carbonate Cores Caused by Alkalis in ASP Flooding in High Salinity/High Temperature Applications. In *Society of Petroleum Engineers - 9th European Formation Damage Conference 2011*; 2011. https://doi.org/10.2118/143155-ms.

(67)   Belhaj, A. F.; Elraies, K. A.; Mahmood, S. M.; Zulkifli, N. N.; Akbari, S.; Hussien, O. S. E. The Effect of Surfactant Concentration, Salinity, Temperature, and PH on Surfactant Adsorption for Chemical Enhanced Oil Recovery: A Review. *J. Pet. Explor. Prod. Technol.* **2020**. https://doi.org/10.1007/s13202-019-0685-y.

(68)   Pantarotto, D.; Singh, R.; McCarthy, D.; Erhardt, M.; Briand, J. P.; Prato, M.; Kostarelos, K.; Bianco, A. Functionalized Carbon Nanotubes for Plasmid DNA Gene Delivery. *Angew. Chemie - Int. Ed.* **2004**. https://doi.org/10.1002/anie.200460437.

(69)   Pastorin, G.; Wu, W.; Wieckowski, S.; Briand, J. P.; Kostarelos, K.; Prato, M.; Bianco, A. Double Functionalisation of Carbon Nanotubes for Multimodal Drug Delivery. *Chem. Commun.* **2006**. https://doi.org/10.1039/b516309a.

(70)   Rai, M.; Ingle, A. P.; Gupta, I.; Brandelli, A. Bioactivity of Noble Metal

Nanoparticles Decorated with Biopolymers and Their Application in Drug Delivery. *International Journal of Pharmaceutics*. 2015. https://doi.org/10.1016/j.ijpharm.2015.10.059.

(71) Arvizo, R. R.; Bhattacharyya, S.; Kudgus, R. A.; Giri, K.; Bhattacharya, R.; Mukherjee, P. Intrinsic Therapeutic Applications of Noble Metal Nanoparticles: Past, Present and Future. *Chem. Soc. Rev.* **2012**. https://doi.org/10.1039/c2cs15355f.

(72) Rasmussen, J. W.; Martinez, E.; Louka, P.; Wingett, D. G. Zinc Oxide Nanoparticles for Selective Destruction of Tumor Cells and Potential for Drug Delivery Applications. *Expert Opinion on Drug Delivery*. 2010. https://doi.org/10.1517/17425247.2010.502560.

(73) Laha, D.; Pramanik, A.; Chattopadhyay, S.; Dash, S. K.; Roy, S.; Pramanik, P.; Karmakar, P. Folic Acid Modified Copper Oxide Nanoparticles for Targeted Delivery in in Vitro and in Vivo Systems. *RSC Adv.* **2015**. https://doi.org/10.1039/c5ra08110f.

(74) Guo, Z.; Zheng, K.; Tan, Z.; Liu, Y.; Zhao, Z.; Zhu, G.; Ma, K.; Cui, C.; Wang, L.; Kang, T. Overcoming Drug Resistance with Functional Mesoporous Titanium Dioxide Nanoparticles Combining Targeting, Drug Delivery and Photodynamic Therapy. *J. Mater. Chem. B* **2018**. https://doi.org/10.1039/c8tb01810c.

(75) Ghosn, Y.; Kamareddine, M. H.; Tawk, A.; Elia, C.; El Mahmoud, A.; Terro,

K.; El Harake, N.; El-Baba, B.; Makdessi, J.; Farhat, S. Inorganic Nanoparticles as Drug Delivery Systems and Their Potential Role in the Treatment of Chronic Myelogenous Leukaemia. *Technology in cancer research & treatment*. 2019. https://doi.org/10.1177/1533033819853241.

(76)　Chen, C.; Wang, S.; Kadhum, M. J.; Harwell, J. H.; Shiau, B. J. Using Carbonaceous Nanoparticles as Surfactant Carrier in Enhanced Oil Recovery: A Laboratory Study. *Fuel* **2018**. https://doi.org/10.1016/j.fuel.2018.03.002.

(77)　Nyankson, E.; Olasehinde, O.; John, V. T.; Gupta, R. B. Surfactant-Loaded Halloysite Clay Nanotube Dispersants for Crude Oil Spill Remediation. *Ind. Eng. Chem. Res.* **2015**. https://doi.org/10.1021/acs.iecr.5b02032.

(78)　Pereira, M. L. D. O.; Maia, K. C. B.; Silva, W. C.; Leite, A. C.; Francisco, A. D. D. S.; Vasconcelos, T. L.; Nascimento, R. S. V.; Grasseschi, D. Fe3O4Nanoparticles as Surfactant Carriers for Enhanced Oil Recovery and Scale Prevention. *ACS Appl. Nano Mater.* **2020**. https://doi.org/10.1021/acsanm.0c00939.

(79)　Villamizar, L.; Lohateeraparp, P.; Harwell, J.; Resasco, D.; Shiau, B. Interfacially Active SWNT/Silica Nanohybrid Used in Enhanced Oil Recovery. In *SPE - DOE Improved Oil Recovery Symposium Proceedings*; 2010. https://doi.org/10.2523/129901-ms.

(80)　Lin, H.; Qu, F.; Wu, X.; Xue, M.; Zhu, G.; Qiu, S. Mixed Surfactants-Directed the Mesoporous Silica Materials with Various Morphologies and Structures. *J.*

Solid State Chem. **2011**, *184* (6), 1415–1420.

https://doi.org/10.1016/j.jssc.2011.03.043.

(81)   Rosestolato, J. C. S.; Pérez-Gramatges, A.; Lachter, E. R.; Nascimento, R. S. V.

Lipid Nanostructures as Surfactant Carriers for Enhanced Oil Recovery. *Fuel*

2019. https://doi.org/10.1016/j.fuel.2018.11.027.

(82)   Sardesai, S.; Biniwale, M.; Wertheimer, F.; Garingo, A.; Ramanathan, R.

Evolution of Surfactant Therapy for Respiratory Distress Syndrome: Past,

Present, and Future. *Pediatr. Res.* **2017**, *81* (1–2), 240–248.

https://doi.org/10.1038/pr.2016.203.

(83)   Pincus, P. Colloid Stabilization with Grafted Polyelectrolytes. *Macromolecules*

1991. https://doi.org/10.1021/ma00010a043.

(84)   Jayaraman, A. Polymer Grafted Nanoparticles: Effect of Chemical and Physical

Heterogeneity in Polymer Grafts on Particle Assembly and Dispersion. *J.*

Polym. Sci. Part B Polym. Phys. **2013**. https://doi.org/10.1002/polb.23260.

(85)   Hwang, Y. K.; Hong, D. Y.; Chang, J. S.; Jhung, S. H.; Seo, Y. K.; Kim, J.;

Vimont, A.; Daturi, M.; Serre, C.; Férey, G. Amine Grafting on Coordinatively

Unsaturated Metal Centers of MOFs: Consequences for Catalysis and Metal

Encapsulation. *Angew. Chemie - Int. Ed.* **2008**.

https://doi.org/10.1002/anie.200705998.

(86)   Bouharras, F. E.; Raihane, M.; Silly, G.; Totee, C.; Ameduri, B. Core-Shell

Structured Poly(Vinylidene Fluoride)-: Grafted -BaTiO 3 Nanocomposites

Prepared via Reversible Addition-Fragmentation Chain Transfer (RAFT) Polymerization of VDF for High Energy Storage Capacitors. *Polym. Chem.* **2019**. https://doi.org/10.1039/c8py01706a.

(87)   Armstrong, J. K.; Meiselman, H. J.; Fisher, T. C. Covalent Binding of Poly(Ethylene Glycol) (PEG) to the Surface of Red Blood Cells Inhibits Aggregation and Reduces Low Shear Blood Viscosity. *Am. J. Hematol.* **1997**. https://doi.org/10.1002/(SICI)1096-8652(199709)56:1<26::AID-AJH5>3.0.CO;2-4.

(88)   Uz, M.; Bulmus, V.; Alsoy Altinkaya, S. Effect of PEG Grafting Density and Hydrodynamic Volume on Gold Nanoparticle-Cell Interactions: An Investigation on Cell Cycle, Apoptosis, and DNA Damage. *Langmuir* **2016**, *32* (23), 5997–6009. https://doi.org/10.1021/acs.langmuir.6b01289.

(89)   Liufu, S.; Xiao, H.; Li, Y. Investigation of PEG Adsorption on the Surface of Zinc Oxide Nanoparticles. *Powder Technol.* **2004**. https://doi.org/10.1016/j.powtec.2004.05.007.

(90)   Zhang, X.; Servos, M. R.; Liu, J. Ultrahigh Nanoparticle Stability against Salt, PH, and Solvent with Retained Surface Accessibility via Depletion Stabilization. *J. Am. Chem. Soc.* **2012**, *134* (24), 9910–9913. https://doi.org/10.1021/ja303787e.

(91)   Williford, J. M.; Archang, M. M.; Minn, I.; Ren, Y.; Wo, M.; Vandermark, J.; Fisher, P. B.; Pomper, M. G.; Mao, H. Q. Critical Length of PEG Grafts on

LPEI/DNA Nanoparticles for Efficient in Vivo Delivery. *ACS Biomater. Sci. Eng.* **2016**. https://doi.org/10.1021/acsbiomaterials.5b00551.

(92) Pasche, S.; Vörös, J.; Griesser, H. J.; Spencer, N. D.; Textor, M. Effects of Ionic Strength and Surface Charge on Protein Adsorption at PEGylated Surfaces. *J. Phys. Chem. B* **2005**. https://doi.org/10.1021/jp050431+.

(93) Buhl, K. B.; Agergaard, A. H.; Møller, R. K.; Kongsfelt, M.; Heide-Jørgensen, S.; Budzik, M. K.; Hinge, M.; Pedersen, S. U.; Daasbjerg, K. Facile Access to Disulfide/Thiol Containing Poly(Glycidyl Methacrylate) Brushes as Potential Rubber Adhesive Layers. *Cite This ACS Appl. Polym. Mater* **2020**. https://doi.org/10.1021/acsapm.0c00306.

(94) Yavuz, E.; Bayramoğlu, G.; Şenkal, B. F.; Arica, M. Y. Poly(Glycidylmethacrylate) Brushes Generated on Poly(VBC) Beads by SI-ATRP Technique: Hydrazine and Amino Groups Functionalized for Invertase Adsorption and Purification. *J. Chromatogr. B Anal. Technol. Biomed. Life Sci.* **2009**. https://doi.org/10.1016/j.jchromb.2009.03.026.

(95) Edmondson, S.; Huck, W. T. S. Controlled Growth and Subsequent Chemical Modification of Poly(Glycidyl Methacrylate) Brushes on Silicon Wafers. *J. Mater. Chem.* **2004**. https://doi.org/10.1039/b312513k.

(96) Xu, Y. S.; Yuan, C. D.; Wang, Y. J.; Cao, T. Y.; Cao, P. Mechanism and Grafting Reactions in Seeded Emulsion Polymerization with Emulsified Monomer Feeding. *J. Appl. Polym. Sci.* **1999**.

https://doi.org/10.1002/(SICI)1097-4628(19990613)72:11<1495::AID-APP11>3.0.CO;2-S.

(97)   Okubo, M.; Hosotani, T.; Yamashita, T.; Izumi, J. Influence of the Swelling State of Seed Polymer Particles with Monomer on the Morphology of Micron-Sized Monodispersed Composite Polymer Particles Produced by Seeded Polymerization Utilizing the Dynamic Swelling Method. *Colloid Polym. Sci.* **1997**. https://doi.org/10.1007/s003960050162.

(98)   Zhu, S.; Hamielec, A. Polymerization Kinetic Modeling and Macromolecular Reaction Engineering. In *Polymer Science: A Comprehensive Reference, 10 Volume Set*; Elsevier, 2012; Vol. 4, pp 779–831. https://doi.org/10.1016/B978-0-444-53349-4.00127-8.

(99)   Park, E. J.; Park, B. C.; Kim, Y. J.; Canlier, A.; Hwang, T. S. Elimination and Substitution Compete During Amination of Poly(Vinyl Chloride) with Ehtylenediamine: XPS Analysis and Approach of Active Site Index. *Macromol. Res.* **2018**, *26* (10), 913–923. https://doi.org/10.1007/s13233-018-6123-z.

(100) Mashat, A.; Abdel-Fattah, A.; Gizzatov, A. NanoSurfactant: A Novel Nanoparticle-Based EOR Approach. In *Society of Petroleum Engineers - SPE Europec featured at 80th EAGE Conference and Exhibition 2018*; 2018. https://doi.org/10.2118/190861-ms.

(101) Pérez-Rodríguez, M.; Prieto, G.; Rega, C.; Varela, L. M.; Sarmiento, F.; Mosquera, V. A Comparative Study of the Determination of the Critical Micelle

Concentration by Conductivity and Dielectric Constant Measurements. *Langmuir* **1998**, *14* (16), 4422–4426. https://doi.org/10.1021/la980296a.

(102)   Barra, G. M. O.; Crespo, J. S.; Bertolino, J. R.; Soldi, V.; Nunes Pires, A. T. Maleic Anhydride Grafting on EPDM: Qualitative and Quantitative Determination. *J. Braz. Chem. Soc.* **1999**, *10* (1), 31–34. https://doi.org/10.1590/S0103-50531999000100006.

(103)   Huang, H.; Hou, L.; Zhu, F.; Li, J.; Xu, M. Controllable Thermal and PH Responsive Behavior of PEG Based Hydrogels and Applications for Dye Adsorption and Release. *RSC Adv.* **2018**, *8* (17), 9334–9343. https://doi.org/10.1039/c8ra01018h.

(104)   Rosi, N. L.; Mirkin, C. A. Nanostructures in Biodiagnostics. *Chem. Rev.* **2005**, *105* (4), 1547–1562. https://doi.org/10.1021/cr030067f.

(105)   Ohnsorg, M. L.; Ting, J. M.; Jones, S. D.; Jung, S.; Bates, F. S.; Reineke, T. M. Tuning PNIPAm Self-Assembly and Thermoresponse: Roles of Hydrophobic End-Groups and Hydrophilic Comonomer. *Polym. Chem.* **2019**, *10* (25), 3469–3479. https://doi.org/10.1039/c9py00180h.

(106)   Musyanovych, A.; Rossmanith, R.; Tontsch, C.; Landfester, K. Effect of Hydrophilic Comonomer and Surfactant Type on the Colloidal Stability and Size Distribution of Carboxyl- And Amino-Functionalized Polystyrene Particles Prepared by Miniemulsion Polymerization. *Langmuir* **2007**, *23* (10), 5367–5376. https://doi.org/10.1021/la0635193.

(107) Johansen, M.; Larsen, C. A Comparison of the Chemical Stability and the Enzymatic Hydrolysis of a Series of Aliphatic and Aromatic Ester Derivatives of Metronidazole. *Int. J. Pharm.* **1985**, *26* (3), 227–241. https://doi.org/10.1016/0378-5173(85)90232-7.

(108) Qin, K.; Yan, Y.; Zhang, Y.; Tang, Y. Direct Production of Levulinic Acid in High Yield from Cellulose: Joint Effect of High Ion Strength and Microwave Field. *RSC Adv.* **2016**, *6* (45), 39131–39136. https://doi.org/10.1039/c6ra00448b.

(109) Jiang, Z.; Fan, J.; Budarin, V. L.; Macquarrie, D. J.; Gao, Y.; Li, T.; Hu, C.; Clark, J. H. Mechanistic Understanding of Salt-Assisted Autocatalytic Hydrolysis of Cellulose. *Sustain. Energy Fuels* **2018**, *2* (5), 936–940. https://doi.org/10.1039/c8se00045j.

(110) Pethes, I.; Bakó, I.; Pusztai, L. Chloride Ions as Integral Parts of Hydrogen Bonded Networks in Aqueous Salt Solutions: The Appearance of Solvent Separated Anion Pairs. *Phys. Chem. Chem. Phys.* **2020**, *22* (19), 11038–11044. https://doi.org/10.1039/d0cp01806f.

(111) Heeb, R.; Lee, S.; Venkataraman, N. V.; Spencer, N. D. Influence of Salt on the Aqueous Lubrication Properties of End-Grafted, Ethylene Glycol-Based Self-Assembled Monolayers. *ACS Appl. Mater. Interfaces* **2009**, *1* (5), 1105–1112. https://doi.org/10.1021/am900062h.

(112) Tasaki, K. Poly(Oxyethylene)-Cation Interactions in Aqueous Solution: A

Molecular Dynamics Study. *Comput. Theor. Polym. Sci.* **1999**, *9* (3–4), 271–284. https://doi.org/10.1016/S1089-3156(99)00015-X.

(113) Speight, J. G. *Transformation of Inorganic Chemicals in the Environment*; 2017. https://doi.org/10.1016/b978-0-12-849891-0.00007-2.

(114) Wan Ngah, W. S.; Hanafiah, M. A. K. M. Removal of Heavy Metal Ions from Wastewater by Chemically Modified Plant Wastes as Adsorbents: A Review. *Bioresource Technology*. 2008, pp 3935–3948. https://doi.org/10.1016/j.biortech.2007.06.011.

(115) Sthoer, A.; Hladílková, J.; Lund, M.; Tyrode, E. Molecular Insight into Carboxylic Acid-Alkali Metal Cations Interactions: Reversed Affinities and Ion-Pair Formation Revealed by Non-Linear Optics and Simulations. *Phys. Chem. Chem. Phys.* **2019**, *21* (21), 11329–11344. https://doi.org/10.1039/c9cp00398c.

(116) Bala, T.; Prasad, B. L. V.; Sastry, M.; Kahaly, M. U.; Waghmare, U. V. Interaction of Different Metal Ions with Carboxylic Acid Group: A Quantitative Study. *J. Phys. Chem. A* **2007**, *111* (28), 6183–6190. https://doi.org/10.1021/jp067906x.

(117) Schramm, L. L. Petroleum Emulsions; 1992; pp 1–49. https://doi.org/10.1021/ba-1992-0231.ch001.

(118) Kogan, A.; Aserin, A.; Garti, N. Improved Solubilization of Carbamazepine and Structural Transitions in Nonionic Microemulsions upon Aqueous Phase

Dilution. *J. Colloid Interface Sci.* **2007**, *315* (2), 637–647.
https://doi.org/10.1016/j.jcis.2007.06.087.

(119) Zhu, T.; Ogbe, D. O.; Khataniar, S. Improving the Foam Performance for
Mobility Control and Improved Sweep Efficiency in Gas Flooding. *Ind. Eng.*
Chem. Res. **2004**, *43* (15), 4413–4421. https://doi.org/10.1021/ie034021o.

(120) Kovscek, A. R.; Bertin, H. J. Estimation of Foam Mobility in Heterogeneous
Porous Media; Society of Petroleum Engineers (SPE), 2002.
https://doi.org/10.2118/75181-ms.

(121) Georgieva, D.; Cagna, A.; Langevin, D. Link between Surface Elasticity and
Foam Stability. https://doi.org/10.1039/b822568k.

(122) Stubenrauch, C.; Hamann, M.; Preisig, N.; Chauhan, V.; Bordes, R. On How
Hydrogen Bonds Affect Foam Stability. *Advances in Colloid and Interface*
Science. Elsevier B.V. September 1, 2017, pp 435–443.
https://doi.org/10.1016/j.cis.2017.02.002.

(123) Schelero, N.; Hedicke, G.; Linse, P.; Klitzing, R. V. Effects of Counterions and
Co-Ions on Foam Films Stabilized by Anionic Dodecyl Sulfate. *J. Phys. Chem.*
B **2010**, *114* (47), 15523–15529. https://doi.org/10.1021/jp1070488.

(124) Buckley, J. S.; Fan, T. *CRUDE OIL/BRINE INTERFACIAL TENSIONS*.

(125) Mahani, H.; Keya, A. L.; Berg, S.; Bartels, W.-B.; Nasralla, R.; Rossen, W. R.
Insights into the Mechanism of Wettability Alteration by Low-Salinity

Flooding (LSF) in Carbonates. **2015**. https://doi.org/10.1021/ef5023847.

(126) Smulders, W.; Monteiro, M. J. Seeded Emulsion Polymerization of Block
Copolymer Core-Shell Nanoparticles with Controlled Particle Size and
Molecular Weight Distribution Using Xanthate-Based RAFT Polymerization.
2004. https://doi.org/10.1021/ma049496l.

(127) Fan, X.; Jia, X.; Zhang, H.; Zhang, B.; Li, C.; Zhang, Q. Synthesis of
Raspberry-Like Poly(Styrene−glycidyl Methacrylate) Particles via a One-Step
Soap-Free Emulsion Polymerization Process Accompanied by Phase
Separation. **2013**. https://doi.org/10.1021/la402759w.

(128) Xu, F.; Zhang, Q.; Gao, Z. Simple One-Step Synthesis of Gold Nanoparticles
with Controlled Size Using Cationic Gemini Surfactants as Ligands: Effect of
the Variations in Concentrations and Tail Lengths. *Colloids Surfaces A
Physicochem. Eng. Asp.* **2013**, *417*, 201–210.
https://doi.org/10.1016/j.colsurfa.2012.10.059.

(129) Zoppe, J. O.; Ataman, C.; Mocny, P.; Wang, J.; Moraes, J.; Klok, A.
Correction: Surface-Initiated Controlled Radical Polymerization: State-of-the-
Art, Opportunities, and Challenges in Surface and Interface Engineering with
Polymer Brushes (Chem. Rev. (2017) 117:3 (1105−1318) DOI:
10.1021/Acs.Chemrev.6b00314). *Chemical Reviews*. American Chemical
Society March 8, 2017, p 4667. https://doi.org/10.1021/acs.chemrev.7b00093.